NASA TN D-327

TECHNICAL NOTE

D-327

A TECHNIQUE FOR DETERMINING RELAXATION TIMES BY FREE-FLIGHT TESTS OF LOW-FINENESS-RATIO CONES; WITH EXPERIMENTAL RESULTS FOR AIR AT EQUILIBRIUM TEMPERATURES UP TO 3440° K

By Jack D. Stephenson

Ames Research Center
Moffett Field, Calif.

NATIONAL AERONAUTICS AND SPACE ADMINISTRATION
WASHINGTON
September 1960

NATIONAL AERONAUTICS AND SPACE ADMINISTRATION

TECHNICAL NOTE D-327

A TECHNIQUE FOR DETERMINING RELAXATION TIMES BY FREE-FLIGHT TESTS OF LOW-FINENESS-RATIO CONES; WITH EXPERIMENTAL RESULTS FOR AIR AT EQUILIBRIUM TEMPERATURES UP TO 3440° K

By Jack D. Stephenson

SUMMARY

This report describes a technique which combines theory and experiments for determining relaxation times in gases. The technique is based on the measurement of shapes of the bow shock waves of low-fineness-ratio cones fired from high-velocity guns. The theory presented in the report provides a means by which shadowgraph data showing the bow waves can be analyzed so as to furnish effective relaxation times.

Relaxation times in air were obtained by this technique and the results have been compared with values estimated from shock tube measurements in pure oxygen and nitrogen. The tests were made at velocities ranging from 4600 to 12,000 feet per second, corresponding to equilibrium temperatures from 3590° R (1990° K) to 6200° R (3440° K), under which conditions, at all but the highest temperatures, the effective relaxation times were determined primarily by the relaxation time for oxygen and nitrogen vibrations.

INTRODUCTION

The effects of molecular vibration and dissociation upon the thermodynamic properties of air (and its constituent gases) at elevated temperatures have been extensively studied, and accurate tabulations of the properties of air have been made at temperatures up to 15,000° K, assuming that the air is in chemical and thermodynamic equilibrium (see refs. 1, 2, and 3). However, when the gas density is low and local velocities are high, or when temperatures vary rapidly along streamlines, the assumption of equilibrium can not necessarily be made, and the rate of adjustment of the gas properties must be taken into account.

It is known that when air is heated suddenly in strong shock waves, the translational and rotational degrees of freedom of the molecules adjust to the new state with essentially no time lag, and that the molecular vibration and dissociation adjust considerably more slowly (ref. 4). When the latter type of adjustments require a time that is of

the same order as the time required for the gas particles to traverse a flow field being studied, it may be important to know accurately the magnitude of this time, since the flow can be significantly influenced by it.

Theories for calculating the variations in gas properties in nonequilibrium flow through normal shock waves have been investigated by various authors: the relaxation of molecular vibrations in oxygen and nitrogen in reference 5; and oxygen dissociation relaxation in references 6, 7, and 8. Reference 5 indicates that the mechanism of the relaxation process for vibrational excitation in a pure gas can be described theoretically. Even for this comparatively uncomplicated process, however, the existing theory does not provide complete information for calculating numerical values of relaxation time, and experimental results are needed to evaluate collision cross-section constants appearing in the theory. At higher enthalpy, when the relaxation involves chemical reactions, and when the gas is a mixture, as in the case of air, the theory is considerably more complex, and is not generally sufficiently precise for use in solving flow problems, where accuracy is essential. Consequently, it is desirable to have available experimental results indicating relaxation times for a wide range of enthalpies and gas densities, for use both in solving engineering problems in gas flow and in evaluating the theory.

The technique that has been employed in obtaining practically all existing relaxation time data at high enthalpy has been to measure in shock tubes the variations with distance or time of the local gas properties in the region just behind the advancing shock wave (see refs. 5, 9, and 10).

This report describes another technique for obtaining relaxation times from experiments which, for certain test conditions, may be more convenient than the shock tube tests. The technique consists in firing from high velocity guns cone-shaped models of low-fineness-ratio and recording the shape of the bow shock wave. Effective relaxation times are then calculated from the wave shape data using a theory developed by D. R. Chapman that is presented in this report.

Tests were conducted to obtain relaxation times in air. At the model velocities of the tests, the enthalpy behind the bow shock waves was such that the nonequilibrium effects were due primarily to the excitation of oxygen and nitrogen vibrations. Relaxation times for vibrations are available from shock-tube tests for these two gases (ref. 5). In the present report, the results from the shock-tube tests in pure oxygen and pure nitrogen were used to estimate effective relaxation times in air, and these times were compared with those determined from the tests described herein.

A limited amount of data was obtained in which small effects of oxygen dissociation could be observed on the bow wave shape. However, such data were not sufficiently precise to permit the calculation of relaxation times for the dissociation.

NOTATION

C_p	pressure coefficient
h	enthalpy
M	Mach number
p	pressure
P	radial coordinate parameter, $\frac{r}{\tau u_o}$
r	radial coordinate
r_b	slant length of cone
R	Reynolds number, also gas constant for unit mass
R_b	model radius
t	temperature ratio across shock wave, $\frac{T_2}{T_1}$, also time
T	absolute temperature
$\overline{T}$	mean temperature, between frozen and equilibrium values
U_1	free-stream velocity
U_2	resultant velocity in region between solid cone and shock wave
u_o	average velocity behind shock wave
u,v	velocity components behind shock wave
v_m	maximum possible velocity, expansion flow
w	resultant velocity just behind the shock wave
y	distance between actual shock wave and reference shock wave (see fig. 2(b))
$\overline{y}$	distance from solid cone surface (see sketch (a))
y_b	distance between shock waves for frozen and equilibrium flow at the distance r_b along model cone (see fig. 2(b))
Z	compressibility factor

α	streamline angle behind shock wave
β	enthalpy ratio divided by temperature ratio, $\frac{h_2/h_1}{T_2/T_1}$
γ	ratio of specific heats for ideal gas
γ_E	effective ratio of specific heats (see eq. (A21))
δ_s	yaw angle of solid cone
δ_w	yaw angle of bow shock wave
δ^*	boundary-layer displacement thickness
θ_w	angular coordinate of bow shock wave
θ_e	bow shock wave angle for equilibrium flow
θ_f	bow shock wave angle for frozen flow
θ_s	solid or model cone half angle
$\Delta\theta$	difference between shock wave angle and solid cone angle, $\theta_w - \theta_s$
ρ	density
σ	increase in apparent shock wave angle due to projection, $\theta_p - \theta_w$
τ	relaxation time

Subscripts

e	equilibrium
E	effective
f	frozen flow
g	oxygen in equilibrium, nitrogen frozen
n	normal shock wave
N	nitrogen
O	oxygen

p	uncorrected for projection effects
s	model cone surface
S	constant entropy
t	parallel to shock wave
w	bow shock wave
o	standard air conditions (1 atm., 59° F), also reference conical flow
1	free stream
2	behind the bow shock wave

METHOD OF EXPERIMENT AND ANALYSIS

The excitation of the internal degrees of freedom in a gas with high total enthalpy is evident as an increase in the specific heat and, when dissociation occurs, also as an increase in the compressibility. The effect of the increased specific heat is to decrease the temperature in the flow behind a shock wave compared with that of an inert gas at the same enthalpy. The density then increases approximately inversely with the temperature, while the pressure in most cases of flow through shock waves is relatively unaffected by the excitation of molecular vibrations and by dissociation. This increased density is opposed to a small extent by the effect of the increased compressibility accompanying dissociation.

In the case of a two-dimensional oblique shock flow, in order to satisfy continuity requirements, the increased density of real air behind the shock wave results in a reduced total stream tube cross section between the shock wave and the solid surface, so that for the same flow turning angle, the shock wave must assume a more acute angle with the flow direction. The same is true for a cone. The geometry of the bow wave on a cone can thus be used as a measure of the state of the air behind the shock wave.

A cone of large included angle is a particularly advantageous model for studying variations in gas properties, because the flow on a cone with an attached shock wave is subject to considerably simpler and more exact analysis than that on most other shapes adaptable to ballistic types of tests, such as blunt bodies with detached shock waves.

A theory which relates the shock wave shape to the thermodynamic properties of the gas is given for cones of large included angle in the following section. It shows that in the case of such cones (selected so

that the flow is everywhere supersonic) the bow shock wave will be conical if the gas is inert or is in equilibrium, and will be curved by a predictable amount when nonequilibrium flow exists.

To provide the experimental shock waves needed for this investigation, conical models of 52.5° and 55° half angle were launched from guns at speeds up to 12,000 feet per second through still air at pressures selected to give frozen, nonequilibrium, and equilibrium flows. The experimental technique is further described in a later section.

Theory

The theory on which the analysis of the tests is based was developed at the Ames Research Center by Dean R. Chapman. Since it has not been published elsewhere, it is presented in this report. This presentation can conveniently be divided into three parts: (1) the calculation of the bow shock wave cone angle for frozen flow, that is, for flow in which the relaxation time is so long that none of the inert degrees of freedom (vibration and dissociation, in this case) are excited, so that the air behaves like a perfect diatomic gas; (2) the calculation of the bow wave angle for flow with the air in equilibrium behind the shock wave, corresponding to a relaxation time of zero; and (3) the calculation of the bow wave shape for nonequilibrium flow with various relaxation times between zero and infinity.

Frozen flow.- Numerical solution of the Taylor-Maccoll equations for flow on an infinite cone furnishes an accurate means of calculating the geometry of the bow wave, as well as the various details of the flow field between the bow wave and the solid cone for frozen flow. In reference 11, such solutions are tabulated for cone angles up to 50°. The approximate method described in appendix A was used to obtain solutions for the slightly larger cone angles required in the studies which are the subject of this report. Figure 1 shows a comparison of the bow wave angles as functions of Mach number calculated for frozen flow by this approximate method and by the exact solution for two infinite solid cones, one having a half cone angle of 50° and on of 55°. In this figure the ordinate $\Delta\theta$ is the difference between the shock wave semicone angle, θ_w, and the solid surface semicone angle, θ_s. It is evident that the bow wave angles obtained in the approximate solution are very nearly the same as those found from the exact calculations.

The exact solution for the 50° cone was obtained from reference 11 in which γ is assumed to be 1.405, whereas for the 55° cone the exact solution was carried out (by Chapman) for a γ of 1.400. The same values of γ were used in the approximate solutions to make these solutions comparable with the exact solutions.

Equilibrium flow.- It is apparent from reference 11 that the numerical solution for the flow on cones is lengthy and time-consuming even when perfect gas relations are employed. If the actual thermodynamic properties of air were included, solving the equations numerically would be considerably more difficult[1] and the solutions would lack generality, so that at any given Mach number, separate solutions would be required for each combination of free-stream temperature and pressure. As a more practicable approach to the problem of calculating the bow wave cone angles and some of the details of the flow behind the bow wave, Chapman investigated the approximate solution presented below. (Two other solutions with similar objectives have been described in refs. 13 and 14.) The solution is presented in terms of an "effective" ratio of specific heats (γ_E) which is related explicitly to the thermodynamic properties of the gas. The solid cones to which the calculations apply are chosen to be as blunt as possible, consistent with the requirement that the bow wave be attached and have a conical shape in equilibrium flow. This bluntness leads to a flow which can be described to a high degree of accuracy considerably more simply than the general cone flow. The assumption is made that the temperature, density, and pressure behind the shock wave are constant in the entire region ahead of the solid cone.

Expressions derived in appendix A relate the density ratio, the bow shock wave angle, and the pressure coefficient behind the shock wave for the flow of a hypothetical gas having a ratio of specific heats that is constant across the shock wave and equal to γ_E. The expressions that relate these variables are the same as those for a perfect gas. Because of the way that γ_E is defined, at any given temperature ratio t, the density ratio ρ_1/ρ_2 determined by equation (A22) for the hypothetical flow is the same as that for the actual flow of the general gas given by equation (A20). Equation (A16), giving the shock wave angle, and equation (A23), giving the pressure coefficient, are the same for the actual flow and the hypothetical flow, and so, since the density ratios are the same, θ_w and C_p are the same in the two flows (for the same solid cone angles and temperature ratios). However, the enthalpy ratios are not the same, and as a result, the Mach numbers of the two flows are different and related by equation (A26).

As the first step in solving specific conical flow problems for the general gas, the solution is obtained for the mathematically simpler hypothetical flow, in terms of the effective γ and the effective Mach number. The solutions corresponding to semicone angles (θ_s) of 52.5° and 55° are shown in figures 3 through 7. With these solutions in

[1]Subsequent to the derivation of relations and the evaluation of the parameters for the cone flows pertaining to this report, reference 12 became available describing the numerical integration of the Taylor-Maccoll equation for equilibrium flow which was programmed on an IBM 704 computer. Such a solution, incorporating the proper free-stream conditions and solid cone angles, had it been available could have been used to obtain the cone-flow parameters required for the studies discussed below.

graphical form, as illustrated, for any assumed conditions which define the states of the gas on each side of the shock wave, γ_E is calculated from equation (A21), and values of M_{1_E}, $\theta_W - \theta_S$, and C_p are read from the graphs. Then, from equation (A26) the free-stream Mach number of the actual flow is obtained, and all of the required quantities have been evaluated for the equilibrium flow.

Appendix B illustrates the calculation of the bow shock wave angle and pressure ratio for a 52.5° solid cone at a free-stream temperature of 540° R at one Mach number and pressure. Results of this and similar calculations for other Mach numbers and pressures are plotted in figure 8 which shows $\Delta\theta$, the difference between the bow shock wave semicone angle and the solid body semicone angle, as a function of Mach number. When oxygen dissociation occurs, the equilibrium bow wave angle is a function of the pressure, as indicated by the lower curves. The latter curves are for constant pressure behind the shock wave.

A2277

Nonequilibrium flow.- In this section an expression is derived from which the coordinates of the bow shock wave on a cone can be calculated for nonequilibrium flow. This flow has the characteristic that the time required for the gas to attain a density near equilibrium, after passing through the shock wave, is of the same order as that required for the gas particles to move a distance typical of the dimensions of the flow field being studied.

In the following development, which first considers an infinite cone, three assumptions are made: (a) the flow properties (ρ, u, h) between the bow wave and cone surface differ by only a small amount from corresponding properties in some reference conical flow (ρ_o, u_o, h_o); (b) this reference conical flow (which could be, e.g., either the frozen conical flow or the equilibrium conical flow) corresponds to a cone angle θ_s sufficiently blunt that all properties ρ_o, u_o, h_o are essentially constant between the bow wave and cone surface; and (c) the free-stream Mach number is sufficiently high that $\theta_w - \theta_s$ is small compared to θ_s (so that $\sin\theta \cong \sin\theta_w$). Referring to the stream tube in sketch (a), from the equality of the free-stream mass flow in, $2\pi\rho_1 u_1 r_w \sin^2\theta_w dr_w$, and the flow out, $2\pi\rho u r \sin\theta \, d\bar{y}$,

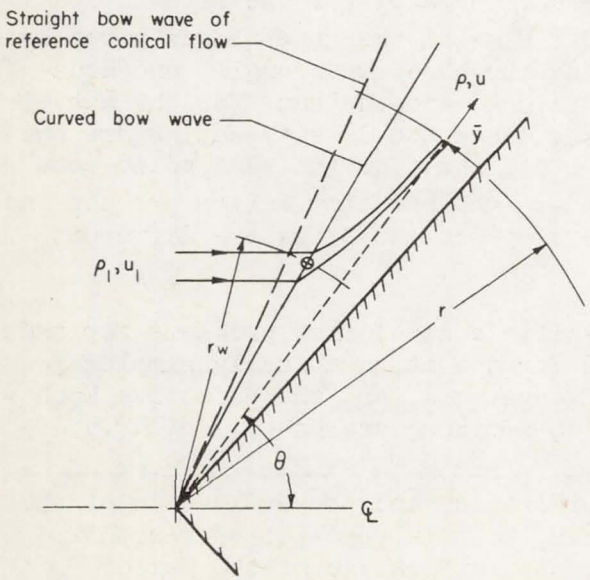

Sketch (a)

and noting that ρu may be expressed as a function of r_w,

$$\int_0^{\bar{y}_w} r \sin\theta \, d\bar{y} = \int_0^r \sin^2\theta_w \frac{\rho_1 u_1}{\rho u} r_w dr_w \qquad (1)$$

By applying this equation first to the nonequilibrium flow, then to the reference conical flow, and subtracting (noting from assumption (c) that $\sin\theta \cong \sin\theta_w \cong \sin\theta_{w_o}$) we have

$$\frac{\rho_o u_o}{\rho_1 u_1} \frac{r}{\sin\theta_{w_o}} \left(\bar{y}_w - \bar{y}_{w_o}\right) = \int_0^r \frac{\rho_o u_o - \rho u}{\rho u} r_w dr_w \qquad (2)$$

For a particle flowing along a streamline the flow properties are regarded as a function of the enthalpy. From assumption (a) of small departures from a reference conical flow,

$$\rho u = \rho_o u_o + \left[\frac{\partial(\rho u)}{\partial h}\right]_o (h - h_o) \qquad (3)$$

equation (2) becomes, upon disregarding second-order terms in the integrand,

$$\frac{\rho_o u_o}{\rho_1 u_1} \left[\frac{\partial h}{\partial(\rho u)}\right]_o \frac{r}{\sin\theta_{w_o}} \left(\bar{y}_w - \bar{y}_{w_o}\right) = \int_0^r \frac{h - h_o}{\rho_o u_o} r_w dr_w \qquad (4)$$

The definition of relaxation time τ is taken as

$$\frac{dh}{dt} = \frac{h_e - h}{\tau} \qquad (5)$$

Since $dh/dt = u\, dh/dr$ along a streamline, this equation for constant τ and constant $u \cong u_o$ (assumptions (b) and (a)) may be integrated between $r = r_w$ and $r = r$ to obtain

$$h_e - h = (h_e - h_w) e^{-(r - r_w)/\tau u_o} \qquad (6)$$

This equation shows that at $r = \infty$, $h = h_e$, as should be the case, and at $r = r_w$, $h = h_w$ (by definition of h_w). By noting that

$$h - h_o = h_e - h_o - (h_e - h)$$

$$= h_e - h_o - (h_e - h_w)e^{-\frac{r - r_w}{\tau u_o}} \tag{7}$$

It follows from equation (4) that, with $x \equiv \frac{r_w}{\tau u_o}$, and $P \equiv \frac{r}{\tau u_o}$,

$$\theta - \theta_o \equiv \frac{\bar{y}_w - \bar{y}_{w_o}}{r} = \frac{C}{P^2}\int_o^P \left(1 - \frac{h_e - h_w}{h_e - h_o}\, e^{x-P}\right) x\, dx \tag{8}$$

Applying this now to the case of a nonequilibrium flow near a reference frozen flow, $h_o = h_f$, and h_w will everywhere be nearly h_f so that equation (8) integrates to

$$\theta - \theta_f = CF(P) \tag{9}$$

where C is a constant equal to $\frac{1}{2}\frac{(h_e - h_f)}{\left(\rho_f u_f\right)^2}\frac{\rho_1 u_1 \sin\theta_f}{\left[\frac{\partial h}{\partial(\rho u)}\right]_f}$

and

$$F(P) \equiv 1 - \frac{2}{P^2}(e^{-P} + P - 1) \tag{10}$$

In the limit of frozen flow $\tau \to \infty$, $P \to 0$, and $F(P) \to (1/3)P$, which gives in the limit, $F(0) = 0$, thus satisfying equation (9). We have

$$\frac{\theta - \theta_f}{\theta_e - \theta_f} = \frac{CF(P)}{\theta_e - \theta_f} \tag{11}$$

so that in the opposite limit of equilibrium flow, $\tau \to 0$, $P \equiv \frac{r}{\tau u_o} \to \infty$, and θ must approach θ_e. We use this requirement to evaluate C from the above equation (noting that $F(\infty) = 1$).

$$1 = \frac{C}{\theta_e - \theta_f} \tag{12}$$

consequently,

$$\frac{\theta - \theta_f}{\theta_e - \theta_f} = F(P) = 1 - \frac{2}{P^2}\left(e^{-P} + P - 1\right) \tag{13}$$

or

$$\frac{\theta - \theta_e}{\theta_f - \theta_e} = \frac{2}{P^2}\left(e^{-P} + P - 1\right) \tag{14}$$

This furnishes an expression from which the coordinates of the bow shock wave on an infinite cone can be calculated when the gas behind the shock wave is not in equilibrium.

$$\frac{\theta_w - \theta_e}{\theta_f - \theta_e} = \frac{2}{(r/\tau u_o)^2}\left(e^{-r/\tau u_o} + \frac{r}{\tau u_o} - 1\right) \tag{15}$$

In this equation θ_w is the angular coordinate and r is the radial distance to points on the shock wave. Also, u_o is the average velocity in the flow behind the shock wave, and τ is the relaxation time. In the derivation presented, τ is the time required for the enthalpy of the gas to reach a specified fraction of its total variation from frozen to equilibrium. If τ is assumed to be a constant during the relaxation, this fraction corresponds to the state when the value of the state parameter deviates by $1/e$ times the initial deviation from the equilibrium value.

It is convenient to alter the form of equation (15) slightly in applying it to the case of finite cones. In this altered form, the distance ratio y/y_b is calculated as

$$\frac{y}{y_b} = \left(\frac{\theta_w - \theta_e}{\theta_f - \theta_e}\right)\frac{r}{r_b}$$

As indicated in figure 2(b), y is the distance measured from the equilibrium shock wave to the curved shock wave at radial distance r, and y_b is the distance between the frozen and equilibrium shock waves at radial distance r_b. This distance ratio y/y_b has been calculated and is shown graphically in figure 9 as a function of the radial coordinate r/r_b for values of the reciprocal relaxation distance ratio $r_b/\tau u_o$ from zero to infinity. At the extreme values of this ratio, zero and infinity, the solutions coincide, respectively, with the solutions for frozen and equilibrium flow behind the shock wave.

Experiments

The theory presented in the preceding sections shows that, from information on the included angle of the bow shock wave of low-fineness-ratio cones, the state of the gas behind the shock wave can be deduced, and in cases where the relaxation adjustments in the gas occur in a portion of the flow which is comparable in size with the region of flow on the conical portion of the model, the relaxation time in the gas can be estimated from the contour of the (curved) shock wave. Experiments were undertaken in which the state parameters of the gas would vary appreciably between the equilibrium and frozen states, and test conditions were selected for which it was expected that nonequilibrium flow would occur. The experiments consisted of launching conical models (of 52.5° and 55° half angle) in free flight at high velocity in the Supersonic Free-Flight Wind Tunnel. The following information was required from the experiments: (1) well-defined pictures of the bow wave from which the wave shape or wave angle could be measured and (2) measurements of the free-stream air properties and the total velocity with which the measured wave geometry could be correlated.

A 2 2 7

Apparatus and models.- The pictures of the bow waves were provided by spark shadowgraphs which are obtained at each of nine instrumented stations in the wind tunnel test section (see ref. 15). For the tests reported, three smooth-bore guns were used to launch the models: a 1-3/4-inch-bore powder gun, a 37-mm light-gas gun, and a caliber 50 light-gas gun. The latter two used helium (compressed in a shock-tube reservoir) as the propellant, as described in reference 15.

The models, examples of which are shown in figure 10, were short blunt cone-cylinders, the forward portions of which were machined from aluminum alloy and were bonded to the cylindrical nylon rear portion with an epoxy resin. (It appeared that screw fastenings between the parts would often promote model breakage in the gun, as a result of stress concentrations.) The flared afterportions of two of the models in figure 10 (which were for use in the light-gas guns) sheared off before the models left the launch tubes.

The models were accurately measured and inspected with a contour projector (at 20× magnification), and only those models were used which had exact straight-sided cones without bluntness or concavity. Slight variations of the included cone angle from the nominal angle were noted, amounting to a maximum of 0.2°, but because of the way in which the data were analyzed, these variations had no effect on the results of the tests.

Tests.- The majority of the data presented in this report has been obtained by firing the models into still air at pressures ranging from 1 atmosphere to 0.057 atmosphere, and at velocities between 7,260 and 12,000 feet per second. In these tests the static temperature of the air was about 530° R.

Tests were also conducted by firing into a supersonic air stream of Mach number 3 in the Supersonic Free-Flight Wind Tunnel, which is described in reference 15. In these tests, for which the air stream static pressure was approximately 0.10 atmosphere and the static temperature was approximately 190° R, data were obtained at Mach numbers from 6.79 to 13.55, corresponding to equilibrium temperatures behind the bow shock wave ranging from 1510° R to 4460° R.

A relatively large number of rounds were fired in the test program but the amount of data obtained was not large, primarily because of two problems: breakage of the model in the launch tube, and oscillations of the model attitude in flight. The oscillations were particularly troublesome when the models were fired into a partial vacuum. In this case the gun muzzle blast often produced a large disturbance to the model attitude, and periods of oscillation were so long that at the instants when the shadowgraphs were recorded, the probability that the model would be at a small angle of attack was low.

Reduction of data.- The data obtained in the tests consisted of the time-distance histories of the model flights, together with spark shadowgraphs at the nine instrumented stations. With (the Mach number 3) air flow in the test section, the free-stream conditions were determined from measured temperatures and pressures in the settling chamber in conjunction with the wind-tunnel calibration.

At each station the angles of yaw and pitch of the models were measured from the shadowgraphs and plotted to reproduce the pitch and yaw histories of the flights. These plots were inspected in order to select the shadowgraphs in which the model was at a sufficiently low angle so that the measured bow wave shapes would be very nearly the same as those for the model at exactly zero angle of attack. As a guide to the maximum permissible angles of attack, the effect of yaw on a conical bow wave was considered. According to references 16 and 17, the bow wave of an infinite cone in flow with constant γ ($\gamma = 1.405$) remains a circular cone with wave angles unchanged even at relatively large angles of yaw. Only a second-order solution indicates a small eccentricity to the circular cone wave shape. Reference 16 also shows that when the solid cone is yawed, the axis of the bow wave cone is generally no longer coincident with the solid cone axis. This is illustrated in figure 11 where the ratios of the yaw angles of these axes are plotted as functions of the solid cone semivertex angle θ_s.

When yawing of the model is moderate and occurs only in the plane parallel to one shadowgraph film plate, the included angle of the bow wave in the shadowgraph is (according to the solution in which γ is constant) the same as that for zero yaw angle.

In addition to the possibility of an aerodynamic effect of yaw, an optical effect is present such that in a plane normal to the plane of yawing, a shadowgraph plate will record the projection on that plane of

the bow wave which has an apparent angle θ_p larger than θ_w according to the relation

$$\tan \theta_p = \frac{\cos \delta \sqrt{\cot^2 \theta_w - \tan^2 \delta}}{\sin^2 \delta - \cos^2 \delta \cot^2 \theta_w}$$

where δ is the yaw angle of the bow wave. The difference between the actual shock-wave cone angle, θ_w and the projected angle, θ_p, $\sigma = \theta_p - \theta_w$, is plotted in figure 12. By the use of figure 11, extrapolated to include model cone angles of 52.5° and 55° and figure 12, it was generally possible to select shadowgraphs from most of the test flights in which the effect of this type of distortion would be less than 0.10°. A correction to the data was applied when the effect of this distortion was significant.

Spark shadowgraphs which showed well-defined bow waves and met the requirements that the model yaw was small were selected and accurately measured. Typical shadowgraphs are shown in figure 13. The coordinates of a series of points along the front of the bow wave image were read parallel and perpendicular to the bisector of the bow wave. A film-reading machine fitted with a microscope was used to measure the coordinates, which could be read to an accuracy of 0.001 inch in the streamwise direction and to 0.005 inch laterally. Figure 14(a) shows an example of the bow wave contour that was read from a shadowgraph in this manner and plotted.

The bow shock waves in the shadowgraphs were not always symmetrical about a bisecting axis, but instead had different curvatures on the two branches. Sometimes the reasons for this asymmetry were not evident, but in other cases it could be attributed qualitatively to the effect of a small yaw angle, which would, in nonequilibrium flow, produce different rates of excitation of the vibrations and dissociation on the two flow regions, the higher temperatures and pressures on the windward side causing a decrease in the relaxation time. Because the theory that has been developed required the assumption that the wave angles are symmetrical, when the bow wave was not symmetrical the curve was oriented symmetrically about the outer portions of the curve (just inside the estimated position where the model shoulder would influence the flow).

To calculate the relaxation time from the bow-wave data, the procedure described below was employed. This calculation is slightly indirect, but it tends to smooth errors in the location of individual points on the bow wave. Coordinates of the points read from the original shadowgraphs were transferred by simple rotation of the axes, so that the outer portion of the bow wave would be symmetrical about the horizontal axis. Polar coordinates of each point were calculated based on a location of the origin at the apex of the bow wave cone. An exact determination of the location of this apex sometimes proved to be the principal factor in limiting the accuracy of the final results. Although the models were

all examined carefully before firing to see that they were truly conical and not blunted or excessively pointed, some of the shadowgraphs evidenced local distortion, refraction effects, fuzziness or other causes of indistinct definition near the apex which would introduce errors. When it appeared that such an error might be large, the shadowgraph involved was not used.

The polar coordinates of the points on the bow wave then were plotted as θ_w as a function of radial distance, r/r_b. This type of plot, shown in figure 14(b), was generally erratic near the origin, at r/r_b less than about 0.3, but became relatively smooth and consistent as the radial coordinates increased to unity. A curve was faired through the portion of the plotted points that defined a consistent relation, treating the upper and lower branches of the bow wave separately. From these two curves, a single mean curve was drawn to represent the best symmetrical average bow wave contour. At two or three values of r/r_b between 0.6 and 1.0, the polar angle θ_w was read from this single curve and y/y_b was computed from the relation

$$\frac{y}{y_b} = \frac{\theta_w - \theta_e}{\theta_f - \theta_e} \frac{r}{r_b}$$

This value of y/y_b, together with the corresponding coordinate r/r_b, locates a point in the graph, figure 9, which determines a value of the parameter $r_b/\tau u_o$. The relaxation time then is

$$\tau = \left(\frac{1}{r_b/\tau u_o} \right) \frac{r_b}{u_o}$$

In this relation u_o is the average particle velocity along a streamline, starting at the shock wave and extending downstream to a point where the gas is close to equilibrium or is leaving the region being considered.

The calculation of an accurate value of u_o is complicated by the necessity of knowing the details of local variations of the state of the air which in turn are functions of relaxation time. Preliminary calculations indicated that the value of u_o obtained assuming that the air reached equilibrium with no time lag would not be greatly different from the value obtained assuming frozen flow with a bow wave angle equal to that for the equilibrium flow. Thus the calculation for the case of frozen flow would correspond to a solution for a more slender solid cone than that of the actual model, but for the same free-stream Mach number. It was estimated that the value of u_o determined in this manner would be accurate within 5 percent. From this it appeared that the degree of approximation involved in using this value of u_o would be well within the accuracy of the measurements for determining values of τ; therefore, this value of u_o was used in reducing all of the data.

Boundary-layer effects.- The possible effects on the bow shock wave shape of the boundary layer on the conical model surface were investigated. In appendix C results of calculations are presented and discussed which show the maximum magnitude of the boundary-layer displacement thickness and the estimated effect on the bow wave angle in conical flow. On the basis of these estimates, it was concluded that the boundary layer had only a very small effect on the bow wave shape in practically all of the tests from which data were derived, and so no correction for this effect was made.

RESULTS AND DISCUSSION

Figures 15(a) through 15(d) show the experimental data that were used in the calculation of the relaxation times. In these figures, as in figure 8, the ordinate $\Delta\theta$ is the difference between the angular (polar) coordinate of points on the shock wave and the half angle of the solid cone. Each pair of symbols joined by a solid line corresponds to a separate shadowgraph. When the two symbols are not coincident, the bow wave had curvature and the wave angle was measured on the shock wave at locations ranging from a point near the apex to a point near the maximum model radius. A total of 20 model shots is represented by the data shown in figure 15.

In addition to the experimental data, figure 15 shows (as in fig. 8) the curves calculated from the theory for frozen flow, flow with the oxygen vibrations fully excited, flow with dissociation frozen, oxygen and nitrogen vibrations fully excited, and flow with vibrations and dissociation in equilibrium.

Figure 15 shows that most of the data lies in the region between the curves for frozen and for fully excited equilibrium flow. From this it is inferred that a major portion of the data contains regions of non-equilibrium flow. Since the data shown were obtained at various free-stream pressures, and since the relaxation time is a function of the local pressure (and the local pressure is a function of the stream pressure), it would not be expected that the data would lie on a continuous curve, unless the flow were either frozen or in equilibrium (without dissociation). The bow wave shapes predicted from the theory and shown in figure 9 indicate that all of the bow waves for nonequilibrium flow become coincident with the wave for frozen flow as the apex is approached. Such coincidence of the maximum values of the wave angles with the values corresponding to frozen flow is not generally evident in the experimental data, primarily because accurate measurement of the wave angles could not be made from the shadowgraphs in the region near the apex (see fig. 14(b)).

In most of the tests, the effect of dissociation was slight, and even at the highest temperatures (i.e., at the highest velocities), dissociation would produce less than a third of the possible variation of θ_w between

frozen and equilibrium at the available range of pressures of the tests: 60 to 5.7 atmospheres behind the shock wave. It became evident that this limited amount of data applicable to oxygen dissociation would be inadequate for the determination of the relaxation time for this process.

Experimental Relaxation Time

Reference 5 presents a discussion of the calculation of vibrational relaxation time from the theory of Landau and Teller (ref. 18) based on general quantum considerations. It is shown that τp, the product of the relaxation time and the pressure of the relaxing gas, is a function of the temperature and of certain characteristics of the gases, including the collision cross sections and the characteristic temperature for vibration. For any one gas then, the theory shows that the relaxation time can be presented as a single curve, τp as a function of temperature. When the results of the tests are presented and compared with shock-tube results in this report, the product τp is therefore used as the relaxation time parameter. In figure 16 it is plotted as a function of the average temperature defined as follows,

$$\overline{T} = \frac{T_e + T_f}{2}$$

where T_e is the calculated equilibrium temperature behind the shock wave and T_f is the temperature calculated assuming frozen flow in which the shock wave angle is the same as the angle in the shadowgraph from which the relaxation time is determined. The relaxation time parameters were obtained from the shadowgraph data as described in the section on reduction of the data. The circular symbols denote the tests in which the models were fired into still air and the triangular symbols denote tests with the models fired into the supersonic air stream of Mach number 3. Symbols joined by vertical lines are from single shadowgraphs which yielded different relaxation times depending upon the radial position along the bow wave that was selected. The data shown were measured at three such positions, at the distances $0.6r_b$, $0.8r_b$, and r_b from the apex outward along the bow wave. Table I provides additional information (such as the local pressures and the equilibrium temperatures) pertaining to the data in figure 16.

The triangular symbols in figure 16 (representing data obtained when the models were fired into the supersonic air stream) shown at temperatures of 1785° K, 1860° K, 2740° K, and 2830° K indicate somewhat longer relaxation times than those predicted, corresponding to larger angles of the bow shock wave than those calculated from the shock tube relaxation time data. A similar result is indicated in table I and figure 15(b) at a Mach number of 6.79 (and a temperature of 830° K) for which the recorded bow shock wave angles were everywhere greater than the cone angle for frozen flow.

Apparently, when the models were fired into the supersonic air stream, the data are influenced by factors other than just the relaxation time.

Data shown in figure 16 and table I at four temperatures (1860°, 2220°, 3550°, and 4030° K) indicate that the value of τ_p varied considerably, depending on the choice of the portion of the bow wave upon which the calculations were based. This large variation corresponds to a large amount of curvature of the bow wave, the cause of which could not be ascertained but which may be partly a result of large yaw angles (up to about 4.4°) that were recorded when some of these shock waves were photographed, and partly a result of inaccuracy due to poor definition of the shock wave in the shadowgraphs. Contributing to the lack of definition were: occasional underexposed pictures resulting in poor photographic contrast; occasional fogging of the film plates by the gun muzzle flash; finite light duration causing a blurred shock wave image; finite size of the spark source which reduced image sharpness.

The remainder of the data obtained with the models launched into still air and one set of data obtained using the supersonic air stream (shown in figure 17 at a temperature of 2090° K), indicate reasonably consistent values of τ_p as a function temperature.

Comparison With Results of Other Tests

Figure 16 also shows the vibrational relaxation times for pure oxygen and pure nitrogen measured in the shock tube tests described in reference 5. It is seen that for nitrogen τ_p is greater than for oxygen by more than an order of magnitude. It would be expected from this that the relaxation of air would not occur as a single process, but instead might be two processes: first, the excitation of the oxygen and an approach to a quasi-equilibrium state in which the nitrogen is almost frozen, and then as the excitation of the nitrogen progressed, an approach more slowly to complete equilibrium. If the processes actually took place separately in this way and if the flow distances were of the proper length, the bow wave shapes would show separate effects which could be identified with each of the two processes. Attempts to identify such effects in the shadowgraphs were not successful, however. The values of τ_p shown in figure 16 for the tests described in this report were calculated as if the relaxation were a single process, and, therefore, τ_p is an effective or apparent relaxation time parameter which characterizes the combined process in air. Since a comparison with shock tube results was considered one of the objectives of the experiments, similar "apparent" relaxation times were calculated from the shock tube data. They are referred to in the following discussion as the predicted relaxation times.

The predicted effective relaxation times in air have been calculated by two methods; in both the air is considered to be a mixture of oxygen (21.4 percent) and nitrogen (78.6), and the assumption is made that the

variation of the state of the gas mixture in the relaxing process is the sum of the variations of the states of component gases, as if they were not mixed. In the first method, which does not depend on the gas flow, the calculated relaxation time is defined as the time required for the mixture to vary its temperature (and density) from frozen to a specified fraction of the total change between frozen and equilibrium. In the second method, the bow shock wave is constructed and an apparent relaxation time is calculated from this shock wave.

In using the first method, it is assumed that the density variations of the oxygen and the nitrogen can be expressed separately as exponential functions of time, so that the variable density of the mixture is given by the following equation.

$$\left(\frac{\rho_M - \rho_{f_M}}{\rho_{e_M} - \rho_{f_M}}\right)\left(\rho_{e_M} - \rho_{f_M}\right) = \left(\rho_{e_0} - \rho_{f_0}\right) e^{-t/\tau_0} + \left(\rho_{e_N} - \rho_{f_N}\right) e^{-t/\tau_N} \tag{16}$$

where the subscript M refers to the gas mixture, 0 refers to oxygen and N to nitrogen. When t is equal to the relaxation time τ_M, $(\rho_M - \rho_{f_M})$ is equal to $1/e(\rho_{e_M} - \rho_{f_M})$, according to the definition of τ that has been mentioned previously. Since the mass fractions of the two component gases are constant, so that

$$\rho_{e_0} = 0.214\ \rho_{e_M}, \qquad \rho_{e_N} = 0.786\ \rho_{e_M}$$

$$\rho_{f_0} = 0.214\ \rho_{f_M}, \qquad \rho_{f_N} = 0.786\ \rho_{f_M}$$

equation (16) may be written

$$0.214\left(e^{-\tau_M p/\tau_0 p}\right) + 0.786\left(e^{-\tau_M p/\tau_N p}\right) = 0.368 \tag{17}$$

If values for $\tau_0 p$ and $\tau_N p$ are taken from the figure 16 (for oxygen vibration and nitrogen vibration, respectively), noting that $\tau_0 p$ is approximately equal to $0.04\ \tau_N p$, equation (17) reduces to the relation

$$\tau_M p = 0.759\ \tau_N p \tag{18}$$

This is shown as the dashed curve in figure 16. Essentially the same relation as equation (18) is obtained if the relaxation time of the oxygen is assumed to be zero.

The predicted relaxation time for air, calculated by the second method is described in detail in appendix D. The shape of a bow shock wave is calculated and from this wave shape, the relaxation time τ and the parameter τp are determined in the same way as in the case of the shock waves obtained experimentally. Results of the calculations are presented in table I and are shown as the rectangular symbols in figure 16. They may be compared with the experimental results shown in this figure at the same temperatures. The variation indicated by the elongation of these rectangular symbols results from calculating the effective τp for several points along the wave. As the location of the point on the shock wave varies, the relative contribution of the oxygen and the nitrogen relaxation processes changes so as to cause a variation in the effective relaxation time parameter.

The shock-tube tests reported in reference 5 provide data for vibrational relaxation time in oxygen only up to a temperature $\overline{T}$ of 3000° K. The results were extended to the higher temperatures indicated in figure 16 by plotting the log of τp as a function of $T^{-1/3}$ (as suggested in ref. 5) and extrapolating. At these high temperatures, the predicted values of τp are quite insensitive to variations of the relaxation time of the oxygen.

The apparent values of τp obtained from the tests would be expected to have the same characteristic as the values predicted by the method involving the construction of a bow shock wave, that is, a variation with the location of the points selected on the shock wave. In addition, these values are also to some extent functions of the pressure and the magnitude of the characteristic flow dimension (i.e., the model size). It appears that for the majority of the points shown, the values of the relaxation time parameter determined experimentally agree fairly well with values calculated by either of the two methods described, in which the results of shock-tube tests in pure oxygen and pure nitrogen are combined to furnish values for relaxation times in air.

In common with most experimental techniques that have been employed to measure relaxation times at high enthalpies, the results obtained in the tests described in this report do not provide precise numerical values for τp. However, in view of the very large differences in the values of this parameter that have resulted from use of various theories for calculating relaxation times for some of the processes involving adjustment rates of the various internal degrees of freedom of a gas, in particular, for dissociation and the other chemical reactions, an experimental method which yields values of τp even within an order of magnitude can be of considerable value. The results shown in figure 16 indicate a mean variation of τp with temperature from which numerical values can be specified well within an order of magnitude.

The tests reported in reference 5 indicated that the vibrational relaxation time of oxygen in a nitrogen mixture was increased because the oxygen-nitrogen collisions are only about 40 percent as effective in transferring energy as are the oxygen-oxygen collisions. If this factor

is included in calculating the effective relaxation times of air, the values of τ for oxygen in air would be about twice those shown in figure 16 for pure oxygen. All of the effective values of τ calculated from the shock-tube results would be increased slightly, but the general comparison of such values with the values obtained from the tests reported herein would not be significantly different from that shown in figure 16, because oxygen is a minor constituent (21 percent) of air.

Results of the tests in still air which covered a range of temperatures ($\overline{T}$) from 1990° to 4260° K and velocities from 7,260 to 12,000 feet per second, indicated values of τp from 60.7 to 0.78 microsecond-atmospheres, corresponding to a range of relaxation times from 4.34 to 0.16 microseconds. At the highest velocities, about 30 percent of the change in bow wave angle between frozen flow and equilibrium is caused by oxygen dissociation, and the relaxation time for the dissociation would have some influence on the effective relaxation time for air calculated from the experimental data. The results thus far obtained, however, are not sufficiently precise to be used to calculate a relaxation time for oxygen dissociation.

Effect of Water Vapor

The effective relaxation time for air is undoubtedly influenced by the presence of gases other than oxygen and nitrogen. Reference 4 indicates that water vapor in ambient air can have an important effect on the relaxation time for oxygen vibrations, because of the much greater effectiveness of oxygen-water molecular collisions compared with oxygen-oxygen and oxygen-nitrogen collisions. The absolute humidity of the air in which models were flown was always about equal to that of ambient air, when the tests were conducted in still air. In these tests it was not feasible to use dry air because there was always some leakage of ambient air into the test section whenever the test section was partially evacuated. It is indicated in reference 5 that an amount of water vapor up to 3 parts in a thousand did not have a measurable effect on the relaxation time in oxygen. In the present tests the amount of water vapor was as much as four times that in the tests reported in reference 5 and may have had some effect. The data have been examined for any consistent relation between the absolute humidity of the ambient air and differences between the predicted and experimentally determined relaxation times. No consistent correlation was evident.

CONCLUSIONS

Conical models of low-fineness-ratio have been tested in free flight at velocities from 4,600 feet per second to 12,000 feet per second, in which the calculated equilibrium temperatures behind the shock wave ranged from 1510° R (840° K) to 6200° R (3440° K) and temperatures in frozen flow

ranged from 1580° R (880° K) to 9140° R (5070° K). Analysis of the results of these tests has led to the following conclusions:

1. The shape of the bow shock wave can be used to calculate a relaxation time in a nonequilibrium flow in the heated region behind the shock wave.

2. Comparison of the relaxation times in air calculated from the present tests with effective relaxation times estimated from results of shock-tube tests with pure oxygen and pure nitrogen indicated that in the temperature range where vibrational relaxation would be expected, these two experimental techniques yield results that agree within the experimental scatter.

Ames Research Center
National Aeronautics and Space Administration
Moffett Field, Calif., May 9, 1960

APPENDIX A

DEVELOPMENT OF APPROXIMATE THEORY FOR CALCULATING EQUILIBRIUM FLOW ON BLUNT CONES

The basic equations of axisymmetric cone flow from reference 11 may be written, with the notation indicated in figure 2(a),

$$\frac{du}{d\theta} - v = 0 \tag{A1}$$

$$\frac{dv}{d\theta} + u + \frac{1}{\rho v}\frac{dp}{d\theta} = 0 \tag{A2}$$

$$\frac{d}{d\theta}(\rho v \sin\theta) + 2\rho u \sin\theta = 0 \tag{A3}$$

Since flow along streamlines is isentropic behind the shock wave, the sonic velocity given by the relation $a^2 = (\partial p/\partial \rho)_S$, may be expressed in the relation

$$\frac{dp}{d\theta} = a^2 \frac{d\rho}{d\theta} \tag{A4}$$

The following expression is obtained by combining the above relations.

$$\frac{1}{a^2}\left(\frac{du}{d\theta}\right)^2\left(\frac{d^2u}{d\theta^2} + u\right) = \frac{d^2u}{d\theta^2} + \frac{du}{d\theta}\cot\theta + 2u \tag{A5}$$

At the solid cone surface, designated by the subscript s, $v_s = 0$, and so from equation (A1), $(du/d\theta)_s = 0$. Equation (A5) at the solid cone surface then becomes

$$\left(\frac{d^2u}{d\theta^2}\right)_s = -2u_s \tag{A6}$$

Expanding v in a series referred to its value on the cone surface, and dropping the higher order terms (assuming $d^2u/d\theta^2$ constant)

$$v = \left(\frac{d^2u}{d\theta^2}\right)_s (\theta - \theta_s) \tag{A7}$$

From equations (A6) and (A7)

$$v = -2u_s(\theta - \theta_s) \tag{A8}$$

Comparison of values obtained from this approximate relation with values given by reference 11 indicates good agreement for the blunt cones considered here. It was noted that even better agreement results if the local radial velocity u is used in equation (A8) instead of the velocity u_s on the surface; that is, defining $\Delta\theta = \theta_w - \theta_s$

$$v_w = -2u_w\Delta\theta \tag{A9}$$

If the velocity ahead of the shock wave, U_1, is resolved into its normal component u_{n_1} and tangential component u_{t_1}, and the velocity behind the shock wave into components u_{n_2} and u_{t_2}, equation (A9), together with oblique wave relations, provides the following:

Since $u_{t_1} = u_{t_2}$ and $v_w = -u_{n_2} = -2u_w\Delta\theta$

$$u_{n_2} = 2u_{t_2}\Delta\theta \tag{A10}$$

$$\tan\theta_w = \frac{u_{n_1}}{u_{t_1}} = \frac{u_{n_1}}{u_{t_2}} \tag{A11}$$

If α is the angle of the streamline deflection through the shock wave,

$$\tan(\theta_w - \alpha) = \frac{u_{n_2}}{u_{t_2}} \tag{A12}$$

$$= \frac{2u_{t_2}\Delta\theta}{u_{t_2}} = 2(\theta_w - \theta_s) \tag{A13}$$

from equations (A10) and (A12). Also, from equations (A11) and (A12)

$$\tan(\theta_w - \alpha) = \frac{u_{n_2}}{u_{n_1}}\tan\theta_w \tag{A14}$$

Then, from equations (A13) and (A14)

$$\frac{u_{n_2}}{u_{n_1}}\tan\theta_w = 2(\theta_w - \theta_s) \tag{A15}$$

Inserting the relation from continuity requirements

$$\frac{u_{n_2}}{u_{n_1}} = \frac{\rho_1}{\rho_2}$$

equation (A15) becomes

$$\left(\frac{\rho_1}{\rho_2}\right) \tan \theta_w = 2(\theta_w - \theta_s) \tag{A16}$$

Equation (A16) relates two of the variables we are most interested in, the wave angle θ_w and the density ratio ρ_1/ρ_2. Since both are unknown we require another relation between them and for this purpose write the momentum and energy equations for flow through the oblique conical shock wave using the normal component of the Mach number M_n and assuming the gas in the free stream is ideal,

$$\frac{p_2}{p_1} = 1 + \left(1 - \frac{\rho_1}{\rho_2}\right) \gamma M_n^2 \tag{A17}$$

$$\frac{h_2}{h_1} = 1 + \left[1 - \left(\frac{\rho_1}{\rho_2}\right)^2\right] \frac{\gamma - 1}{2} M_n^2 \tag{A18}$$

The equation of state may be written

$$\frac{p_2}{p_1} = \frac{t\rho_2}{\rho_1} Z_2 \tag{A19}$$

where $t = T_2/T_1$ and Z_2 is the compressibility, $p_2/\rho_2 RT_2$. Equations (A17), (A18), and (A19) may be combined to give the relation

$$\left(\frac{\rho_1}{\rho_2}\right)^2 + \frac{\rho_1}{\rho_2}\left[\frac{2\gamma}{\gamma - 1}(\beta t - 1) - (tZ_2 - 1)\right] - tZ_2 = 0 \tag{A20}$$

where $\beta = (h_2/h_1)(T_1/T_2)$. If an effective ratio of specific heats, γ_E, is defined by the relation

$$\frac{\gamma_E + 1}{\gamma_E - 1} = \frac{\gamma + 1}{\gamma - 1} + \frac{t}{t - 1}\left[(\beta - 1)\frac{2\gamma}{\gamma - 1} - (Z_2 - 1)\left(1 + \frac{\rho_2}{\rho_1}\right)\right] \tag{A21}$$

equation (A20) becomes

$$\left(\frac{\rho_1}{\rho_2}\right)^2 + \frac{\rho_1}{\rho_2}\left[\frac{\gamma_E + 1}{\gamma_E - 1}(t - 1)\right] - t = 0 \qquad \text{(A22)}$$

It may be noted that in the special case of a perfect gas ($\beta = 1$, $Z_2 = 1$), the definition of γ_E, equation (A21), reduces to $\gamma_E = \gamma$. Neither β nor Z appears in equation (A22), which is the same as the expression for the density ratio in a perfect gas having $\gamma = \gamma_E$, and the same value of t.

An expression for the pressure is found by writing the momentum equation for the normal component across the shock wave

$$p_1 - p_2 = \rho_1 u_{n_1}^2 - \rho_2 u_{n_2}^2$$

From continuity,

$$\rho_1 u_{n_1} = \rho_2 u_{n_2}$$

so that

$$\frac{p_1 - p_2}{\rho_1 u_{n_1}^2} = 1 - \frac{\rho_1}{\rho_2}$$

Since, by definition,

$$C_p = \frac{p_2 - p_1}{(1/2)\rho_1 U_1^2}$$

and

$$u_{n_1} = U_1 \sin \theta_w$$

The pressure coefficient may be expressed as follows:

$$C_p = 2 \sin^2\theta_w \left[1 - (\rho_1/\rho_2)\right] \qquad \text{(A23)}$$

In the hypothetical flow, the enthalpy ratio is equal to the temperature ratio. Putting $t = h_2/h_1$ and $M_{n_E} = M_{1_E} \sin \theta_w$ into equation (A18),

A 2 2 7

$$M_{1_E}^2 \sin^2\theta_w = \frac{t - 1}{\left[1 - (\rho_1/\rho_2)^2\right](1/2)(\gamma_E - 1)} \tag{A24}$$

Writing equation (A18) for the general gas with $h_2/h_1 = \beta t$,

$$M_1^2 \sin^2\theta_w = \frac{\beta t - 1}{\left[1 - (\rho_1/\rho_2)^2\right](1/2)(\gamma - 1)} \tag{A25}$$

The Mach numbers of the two flows are related by the following equation, obtained by combining equations (A24) and (A25).

$$M_1 = M_{1_E}\left[\frac{(\beta t - 1)}{(t - 1)}\,\frac{(\gamma_E - 1)}{(\gamma - 1)}\right]^{1/2} \tag{A26}$$

APPENDIX B

EXAMPLE CALCULATION

This appendix presents an example of the calculation of the bow shock wave angle θ_w and the pressure ratio across the shock for a 52.5° cone. The temperature and pressure behind the shock wave are assumed to be, respectively, 3800° K (6840° R) and 10 atmospheres, and a free-stream temperature of 300° K (540° R) is selected. The enthalpies and compressibility factor for air obtained from references 1 and 3 were as follows for the assumed conditions.

$$h_1 = 3.83\ RT_o$$

$$h_2 = 74.1\ RT_o$$

$$Z_2 = 1.066$$

From equation (A20), $\rho_1/\rho_2 = 0.1179$. From equation (A21), assuming $\gamma = 1.405$, the value $\gamma_E = 1.244$ is obtained. For this value of γ_E and $0.3t = 0.3(T_2/T_1) = 0.3(3800/300) = 3.8$, figure 3 gives the the effective Mach number

$$M_E = 11.62$$

With this M_E, equation (A26) gives the stream Mach number

$$M_1 = 11.29$$

From figure 4 and the above values of γ_E and M_E,

$$\Delta\theta = 5.50$$

The bow shock wave angle is

$$\theta_w = \theta_s + \Delta\theta$$

$$= 52.5 + 5.50$$

$$= 58.00$$

Obtaining the pressure coefficient from figure 7,

$$C_p = 1.266$$

This together with the assumed pressure behind the shock wave permits the calculation of a pressure ratio and a stream static pressure

$$\frac{p_2}{p_1} = 1 + \frac{C_p M_1^2 \gamma}{2}$$

$$= 1 + \frac{(1.266)(11.29)^2(1.405)}{2}$$

$$= 113.4$$

$$p_1 = p_2/(p_2/p_1) = 10/113.4$$

$$= 0.0882 \text{ atmosphere}$$

APPENDIX C

EFFECT OF THE BOUNDARY LAYER ON THE SHOCK-WAVE SHAPE

The magnitude of the change in the shock-wave shape due to the boundary layer would depend on the condition of the boundary layer. In some of the tests, it was possible to determine whether the boundary layer was laminar or turbulent by inspection of the shadowgraphs. Such tests indicated that in most cases the boundary layer was entirely laminar; however, turbulent boundary layers were observed in a few cases, and the possibility existed that the boundary layers were turbulent in some of the tests for which it was not possible to determine their condition from the shadowgraphs. In order to establish the limits of the possible effects, the maximum effects of laminar and turbulent boundary layers on the shock wave shapes were calculated.

From heat-transfer calculations (and also from experimental results) it can be shown that the model surface temperatures in tests such as those discussed in this report are always considerably lower than the adiabatic wall temperature, because of the short duration of the tests and the high conductivity of the model. In calculating the thickness of the laminar boundary layer, the effect of heat transfer to the model surface has been taken into account by use of the results presented in reference 19. In this reference, theoretical results are given for an assumed ratio of wall temperature to temperature outside the boundary layer of 0.25. In most of the tests, the temperature ratio was estimated to be even smaller than this, but this ratio is typical of the test conditions for which the boundary-layer thickness was maximum. In addition to assuming that the temperature ratio of 0.25 would be applicable, a combination of conditions was selected in which other factors would cause the boundary-layer thickness to be large, and the boundary-layer thickness was calculated for this one case to determine the maximum effect of the laminar boundary layer. For this combination of conditions, the Reynolds number behind the bow shock wave was 0.9 million per inch, or a Reynolds number of one million, based on the slant length of the cone. (The Reynolds number based on the stream conditions was 1.7 million per inch.)

The thickness of the boundary layer on a cone was related to that on a flat plate by the relation

$$\delta^*_{\text{cone}} = \left(\sqrt{3/2}\right) \delta^*_{\text{plate}}$$

which results from the rule (given, e.g., in ref. 20) that the skin friction on a cone is $\sqrt{3}$ times the value for a flat plate. The boundary-layer displacement thickness at the most rearward location on

the conical surface was calculated to be 0.00053 inch, corresponding to an effective angular change in the model cone half angle of 0.025°. This change in the effective model cross section would produce a negligible change in the shape of the bow shock wave. Although the way in which the effect of heat transfer is taken into account is not exact insofar as the surface temperature of the model is not known, if the effect were entirely disregarded, the calculated thickness of the laminar boundary layer would be no more than twice the value obtained when wall cooling was assumed and might still be neglected within the accuracy of the measurements.

To estimate the maximum effect of a turbulent boundary layer, as in the case of the laminar boundary layer, calculations were made for one combination of conditions in which the displacement thickness might be expected to be a maximum. The same Reynolds number was selected as in the case of the laminar boundary layer. The thickness of a turbulent boundary layer on a cone was calculated by an unpublished method in which the effect of heat transfer can be taken into account if the effect of heat transfer on the skin-friction coefficient is known. The skin friction for flow with heat transfer was computed by the method described in reference 21. For the conditions considered, the maximum calculated displacement thickness was 0.0016 inch. The effective increase in the cross section of the model cone corresponds to an increase in the solid cone angle (in the region where shadowgraph data were measured) of about 0.12°. The influence of this incremental cone angle on the bow shock wave angle is indicated in figure 17, which shows the bow wave angle as a function of cone angle for frozen flow at Mach numbers of 6, 10, and infinity, and for equilibrium flow at Mach numbers of 6 and 10. The maximum slope of these curves, for the range of conditions of the tests, was 2.2. This indicates that the angular coordinate of the bow wave could increase by 0.26°, if the model has a turbulent boundary layer originating at the apex of the cone. This increase would have some effect, such as to increase the calculated value of the relaxation time, that would increase with a decreasing difference between $\Delta\theta_f$ for frozen flow and $\Delta\theta_e$ for equilibrium flow. The largest effect then occurs at the lower model velocities, and for the smaller solid cone angles.

Because this value of the angular increment, 0.26°, results from a combination of assumed conditions such as to produce the maximum effect, and because it is believed that in most of the tests the boundary layer was partly or entirely laminar so that the effect would be much smaller, no correction was made for the effect of the boundary layer on the shape of the bow shock wave.

APPENDIX D

PREDICTED EFFECTIVE VIBRATIONAL RELAXATION TIMES

BASED ON A CALCULATED SHOCK-WAVE SHAPE

The second of the two methods employed in this report to calculate the predicted relaxation times for air is presented in this appendix. First, relations are obtained from which the bow wave shape can be calculated, and then the relaxation times are calculated from this wave shape. Calculations are made for conditions selected so that the results can be compared directly with each set of experimental results.

The following equation is assumed to specify the time variation of temperature of the air as it approaches equilibrium after having been heated as an inert gas by the shock wave.

$$T - T_e = (T_f - T_g)e^{-t/\tau_O} + (T_g - T_e)e^{-t/\tau_N} \tag{D1}$$

where the subscript g refers to the state of the gas corresponding to oxygen in equilibrium while the nitrogen remains frozen. Introducing the density and pressure from the equation of state into equation (D1)

$$\frac{p}{\rho R} - \frac{p_e}{\rho_e R} = \left(\frac{p_f}{\rho_f R} - \frac{p_g}{\rho_g R}\right) e^{-t/\tau_O} + \left(\frac{p_g}{\rho_g R} - \frac{p_e}{\rho_e R}\right) e^{-t/\tau_N} \tag{D2}$$

At any given free-stream Mach number, it can be shown that the pressure ahead of a blunt body is not a sensitive function of the gas state, in which case it can be assumed that p, p_e, and p_t are equal. Also, with no dissociation, the gas constants are equal. Equation (D2) can then be written

$$\frac{1}{\rho} - \frac{1}{\rho_e} = \left(\frac{1}{\rho_f} - \frac{1}{\rho_g}\right) e^{-t/\tau_O} + \left(\frac{1}{\rho_g} - \frac{1}{\rho_e}\right) e^{-t/\tau_N} \tag{D3}$$

It is now desirable to relate the bow shock wave geometry to the density. The shock wave angle is given as a function of density in equilibrium flow by equation (A16), which can be written

$$\frac{1}{\rho_2} = \frac{2}{\rho_1} \frac{\Delta\theta}{\tan \theta_w} \tag{D4}$$

Putting equation (D4) into equation (D3) and observing that ρ_1, the free stream density, is the same in each term,

$$\frac{\Delta\theta}{\tan\theta_w} - \frac{\Delta\theta_e}{\tan\theta_e} = \left(\frac{\Delta\theta_f}{\tan\theta_f} - \frac{\Delta\theta_g}{\tan\theta_g}\right) e^{-t_a/\tau_0} + \left(\frac{\Delta\theta_g}{\tan\theta_g} - \frac{\Delta\theta_e}{\tan\theta_e}\right) e^{-t_a/\tau_N} \tag{D5}$$

For this expression to have a meaning, it is necessary to assume that an average effective density can be defined which is related by equation (D4) to the angular coordinates of points on the shock wave in nonequilibrium flow. This density is, in general, a function of the radial coordinate. In equation (D5) the time t_a is the time required for a small volume of gas to attain the average effective density as it moves downstream from the shock wave.

To determine whether it is possible to assume that an effective average density and a corresponding flow time t_a can actually be defined, equation (D4) was applied to a nonequilibrium flow, assuming that the gas undergoes only a single relaxation toward equilibrium. The result was compared with the result obtained using the derived relations for nonequilibrium flow and figure 9. The purpose of this comparison was to see if any value of t_a would bring the results into agreement. It was found that relatively good agreement is obtained (at least for the case of model cone angles of 52.5° and 55°) if t_a is taken as $0.2(r_b/u_o)$.

Equation (D5) was then used with this value of t_a to calculate $\Delta\theta/\tan\theta_w$ for three radial locations on the shock wave, $0.6r_b$, $0.8r_b$, and r_b. For each of these values of $\Delta\theta/\tan\theta_w$, the angular coordinate θ_w was calculated and y/y_b was computed:

$$\frac{y}{y_b} = \frac{\theta_w - \theta_e}{\theta_f - \theta_e}\frac{r}{r_b}$$

The relaxation time ratio $r_b/\tau u_o$ was determined from figure 9 and converted into the parameter τp using the same values of r_b, u_o, and p as those used in reducing the corresponding experimental results.

REFERENCES

1. Hilsenrath, Joseph, et al.,: Tables of Thermal Properties of Gases. National Bureau of Standards Circular 564 (1955), Supt. of Documents, Washington 25, D. C.

2. Hilsenrath, Joseph, and Beckett, Charles W.: Tables of Thermodynamic Properties of Argon-Free Air to 15,000° K. AEDC TN-56-12, 1956.

3. Feldman, Saul: Hypersonic Gas Dynamic Charts for Equilibrium Air. AVCO Res. Lab., Jan., 1957.

4. Bethe, H. E., and Teller, E.: Deviations from Thermal Equilibrium in Shock Waves. Rep. No. X-117, Ballistic Res. Lab., Aberdeen Proving Ground, Md., 1945.

5. Blackman, Vernon: Vibrational Relaxation in Oxygen and Nitrogen. Jour. Fluid Mech., vol. 1, pt. 1, May 1956, pp. 61-85.

6. Wood, George P.: Calculations of the Rate of Thermal Dissociation of Air Behind Normal Shock Waves at Mach Numbers of 10, 12, and 14. NACA TN 3634, 1956.

7. Evans, John J.: Method for Calculating Effects of Dissociation on Flow Variables in the Relaxation Zone Behind Normal Shock Waves. NACA TN 3860, 1956.

8. Heims, Steve P.: Effect of Oxygen Recombination on One-Dimensional Flow at High Mach Numbers. NACA TN 4144, 1958.

9. Resler, E. L., Jr., and Scheibe, M.: An Instrument to Study Relaxation Rates Behind Shock Waves. Univ. of Maryland, Tech. Note BN-39, Aug. 1954.

10. Camac, M., Camm, J., Keck, J., and Petty, C.: Relaxation Phenomena in Air Between 3000° and 8000° K. AVCO Res. Lab. Rep. 22, March 13, 1958.

11. Staff of the Computing Section (under the direction of Zdenek Kopal): Tables of Supersonic Flow Around Cones. Tech. Rep. 1, Center of Analysis, M.I.T., Cambridge, 1947.

12. Romig, Mary F.: Conical Flow Parameters for Air in Dissociation Equilibrium: Final Results. Convair Res. Note 14, Jan. 1958.

13. Hayes, Wallace D.: Some Aspects of Hypersonic Flow. Ramo-Wooldridge Corp., Jan. 4, 1955.

14. Feldman, Saul: Hypersonic Conical Shocks for Dissociated Air in Thermodynamic Equilibrium. AVCO Res. Lab., Rep. 12, May 1957. (Also Jet Propulsion, vol. 27, no. 12, May 1957, pp. 1253-55.

15. Seiff, Alvin: The Use of Gun-Launched Models for Experimental Research at Hypersonic Speeds. AGARD Rep. 138, July 1957.

16. Staff of the Computing Section (under the direction of Zdenek Kopal): Tables of Supersonic Flow Around Yawing Cones. Tech. Rep. 3, Center of Analysis, M.I.T., Cambridge, 1947.

17. Staff of the Computing Section (under the direction of Zdenek Kopal): Tables of Supersonic Flow Around Cones of Large Yaw. Tech. Rep. 5, Center of Analysis, M.I.T., Cambridge, 1949.

18. Landau, L, and Teller, E.: On the Theory of Sound Dispersion. Physikalische Zeitschrift der Sowjetunion, v. 10, 1936, pp. 34-43.

19. Van Driest, E. R.: Investigation of the Laminar Boundary Layer in Compressible Fluids Using the Crocco Method. NACA TN 2597, 1952.

20. Shapiro, Ascher H.: The Dynamics and Thermodynamics of Compressible Fluid Flow. The Ronald Press Co., New York, Vol. II, 1953, p. 1067.

21. Sommer, Simon C., and Short, Barbara J.: Free-Flight Measurements of Turbulent-Boundary-Layer Skin Friction in the Presence of Severe Aerodynamic Heating at Mach Numbers From 2.8 to 7.0. NACA TN 3391, 1955.

TABLE I.- TEST CONDITIONS AND RELAXATION TIME PARAMETERS

	M_1	T_1, °R	T_{2_e}, °R	$\bar{T}$, °R	$\bar{T}$, °K	Pressure behind shock P_2, atm	Average velocity behind shock u_o, ft/sec	θ_s, deg	Model reference length r_b, ft	Radial coordinate r/r_b	τ_p, experiment μsec-atm	τ_p, predicted μsec-atm	$\frac{\tau_p(\text{experimental})}{\tau_p(\text{predicted})}$
Still air tests	6.48	522	3360	3590	1990	38.9	3610	52.7	0.0762	0.6	48.3	33.6	1.43
										.8	41.7	27.9	1.49
										1.0	42.0	14.0	3.00
	6.53	536	3500	3757	2085	16.0	3630	52.5	.0264	.6	40.5	24.5	1.65
										.8	32.6	27.4	1.19
										1.0	51.0	28.0	1.82
	6.82	526	3630	3890	2220	45.0	3900	52.4	.0264	.6	55.8	42.7	1.31
										.8	32.0	45.9	.70
										1.0	7.2	45.9	.16
	6.91	536	3800	4150	2305	18.2	3940	52.5	.0264	.6	16.2	24.9	.65
										.8	13.9	29.3	.47
										1.0	15.6	30.6	.51
	7.24	525	4400	4650	2580	51.5	3700	55.0	.0737	.6	41.1	20.5	2.00
										.8	54.8	18.4	2.98
										1.0	59.2	8.2	7.23
	7.39	532	4180	4540	2520	14.0	4160	52.5	.0264	.6	46.0	21.8	2.11
										.8	29.4	23.9	1.23
										1.0	60.7	26.2	2.32
	7.69	530	4380	4775	2650	55.0	4430	52.6	.0264	.6	49.8	29.5	1.69
										.8	34.2	32.8	1.04
										1.0	56.0	32.8	1.71
	7.90	532	4580	5025	2790	16.0	4620	52.5	.0264	.6	22.5	20.2	1.11
										.8	21.3	25.6	.83
										1.0	36.0	24.6	1.46
	8.15	537	4780	5280	2930	23.6	4770	52.5	.0264	.6	13.0	21.1	.62
										.8	31.2	22.4	1.39
										1.0	36.8	26.9	1.37
	8.97	536	5420	6100	3390	19.0	5340	52.5	.0264	.6	16.7	16.9	.99
										.8	6.6	17.8	.37
										1.0	9.4	17.8	.53
	9.07	532	5370	6195	3440	7.9	5280	52.6	.0264	.6	14.6	10.9	1.34
										.8	17.2	12.6	1.37
										1.0	20.2	14.6	1.38
	9.08	536	5480	6230	3460	19.0	5370	52.5	.0264	.6	8.6	16.4	.52
										.8	12.5	16.8	.74
										1.0	24.4	17.8	1.37
	9.23	538	5630	6415	3560	11.0	5460	52.5	.0264	.6	3.8	12.5	.30
										.8	8.1	14.1	.57
										1.0	10.8	14.8	.73
	9.34	527	5450	6385	3550	5.7	5380	52.5	.0264	.6	80.0	8.89	9.00
										.8	9.0	9.80	.09
										1.0	---	5.70	---
	10.27	522	6160	7250	4030	17.0	6190	52.5	.0264	.6	2.6	10.8	.25
										.8	9.9	10.9	.91
										1.0	15.8	10.2	1.55
	10.56	535	6180	7610	4230	5.0	6410	52.5	.0264	.6	.78	5.35	.15
										.8	1.14	5.75	.20
										1.0	1.43	6.10	.23
	10.58	534	6200	7670	4260	5.9	6330	52.5	.0264	.6	9.31	7.02	1.33
										.8	7.03	7.67	.92
										1.0	9.20	8.02	1.15
Mach 3 air stream	6.79	193	1510	1545	860	4.5	2180	52.6	.0920	.6	∞	112.0	∞
										.8	∞	121.0	∞
										1.0	∞	129.0	∞
	7.33	196	1740	1780	990	7.0	2420	52.6	.0920	.6	∞	85.4	∞
										.8	442	86.1	5.13
										1.0	174	97.3	1.79
	10.73	186	3020	3215	1785	13.3	3570	52.5	.0762	.6	151	58.1	2.60
										.8	151	72.2	2.09
										1.0	159	87.2	1.82
	10.99	186	3140	3345	1860	13.9	3680	52.5	.0762	.6	594	56.4	10.5
										.8	90	65.6	1.37
										1.0	---	71.7	---
	11.25	188	3560	3760	2090	15.2	3460	55.0	.0737	.6	50.5	55.0	.92
										.8	34.4	65.4	.53
										1.0	44.4	69.6	.64
	13.55	193	4460	4935	2740	17.6	4750	52.5	.0762	.6	57.0	32.0	1.78
										.8	73.3	33.8	2.17
										1.0	78.0	30.8	2.53
	13.84	191	4550	5095	2830	20.5	4730	52.6	.0264	.6	37.2	23.4	1.59
										.8	79.2	26.9	2.94
										1.0	87.9	28.7	3.06

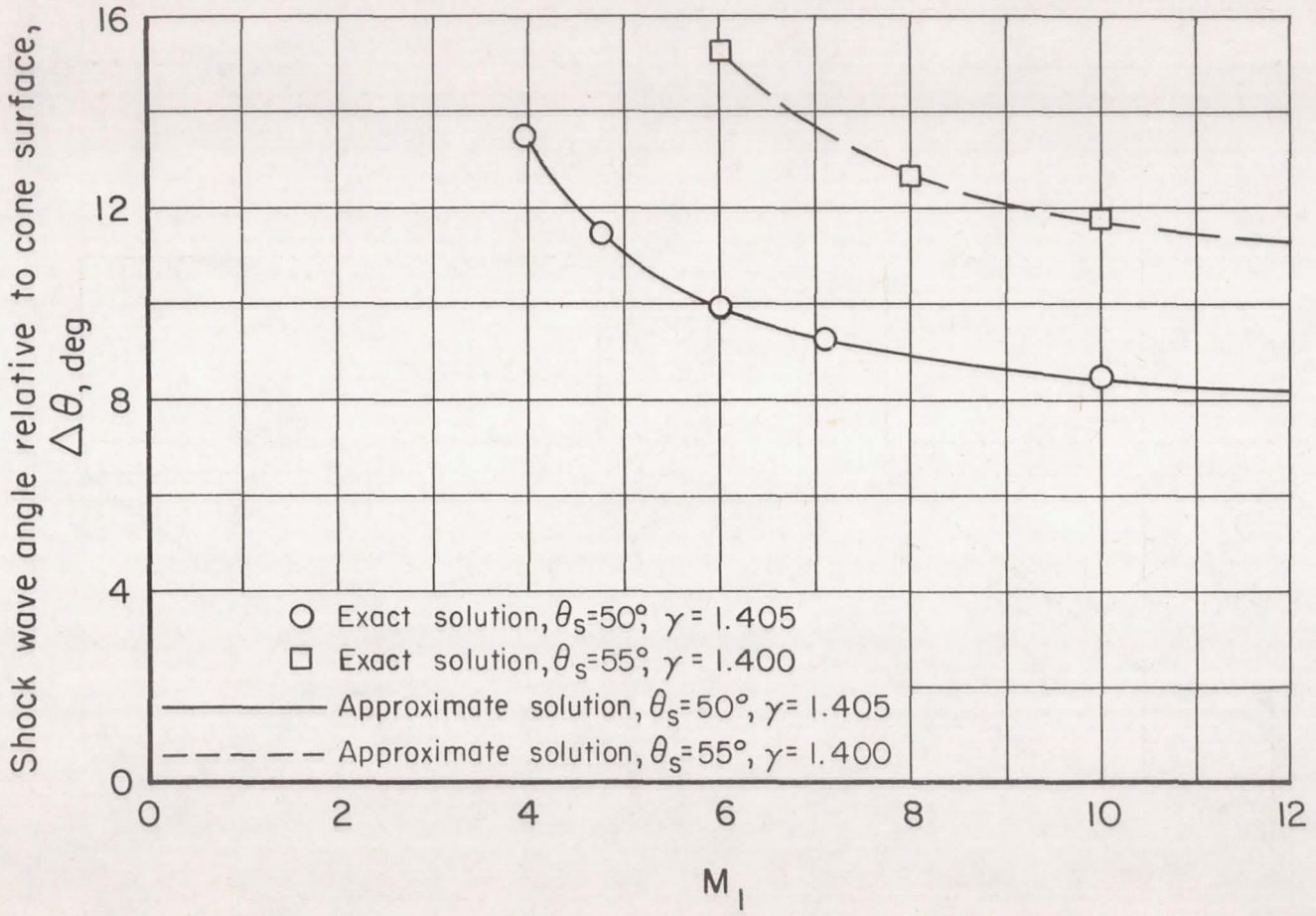

Figure 1.- Comparison of the calculated bow shock wave angles from approximate theory with the wave angles from exact theory; frozen flow.

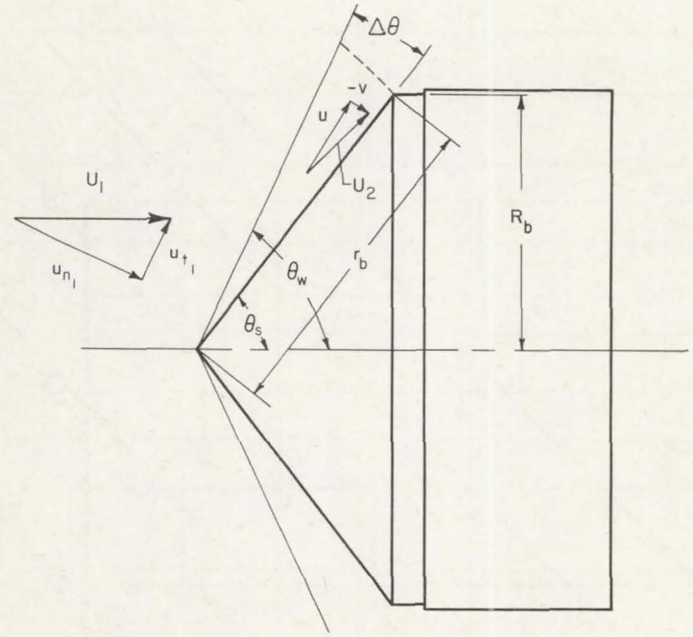

(a) Equilibrium flow.

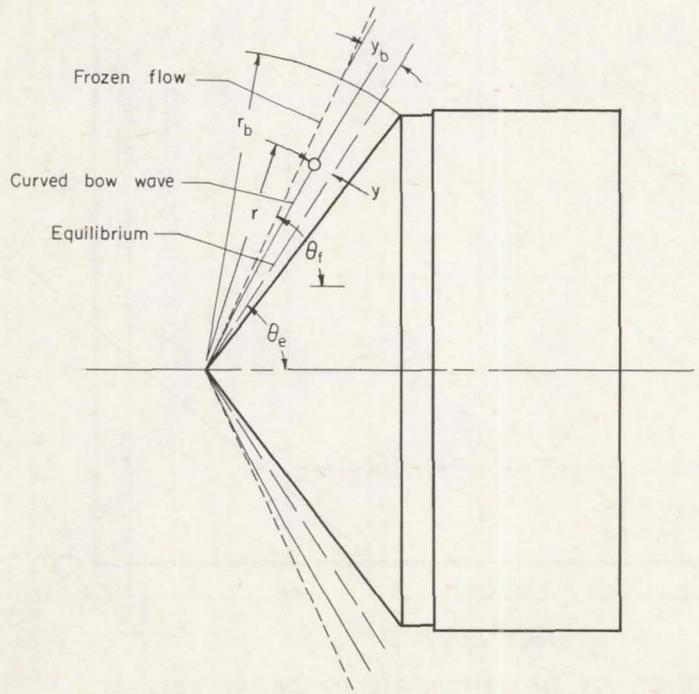

(b) Nonequilibrium flow.

Figure 2.- Sketch showing model geometry and flow field notation.

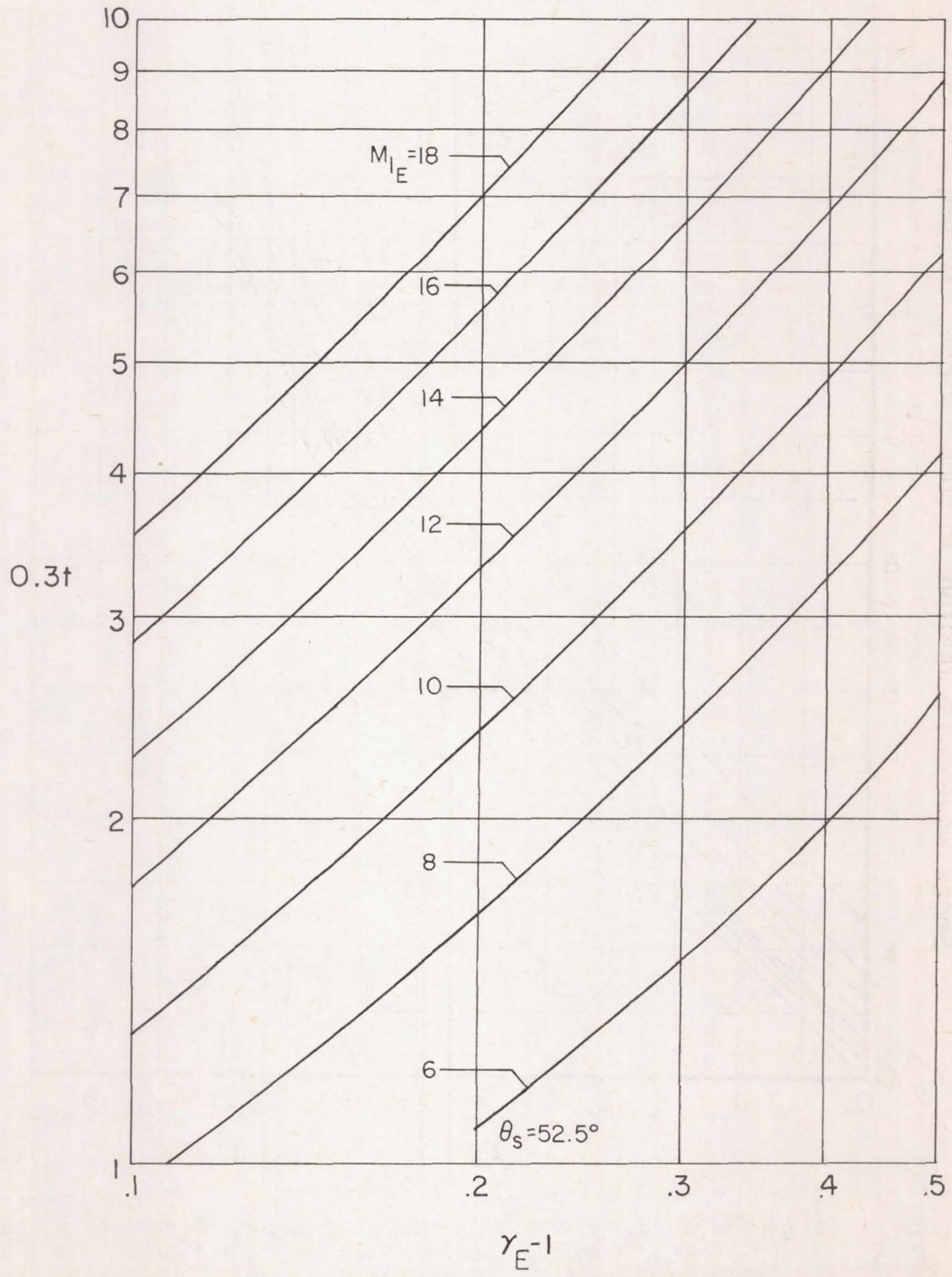

Figure 3.- Graph showing relation between temperature ratio t, effective γ, and effective Mach number; $\theta_s = 52.5^{\circ}$.

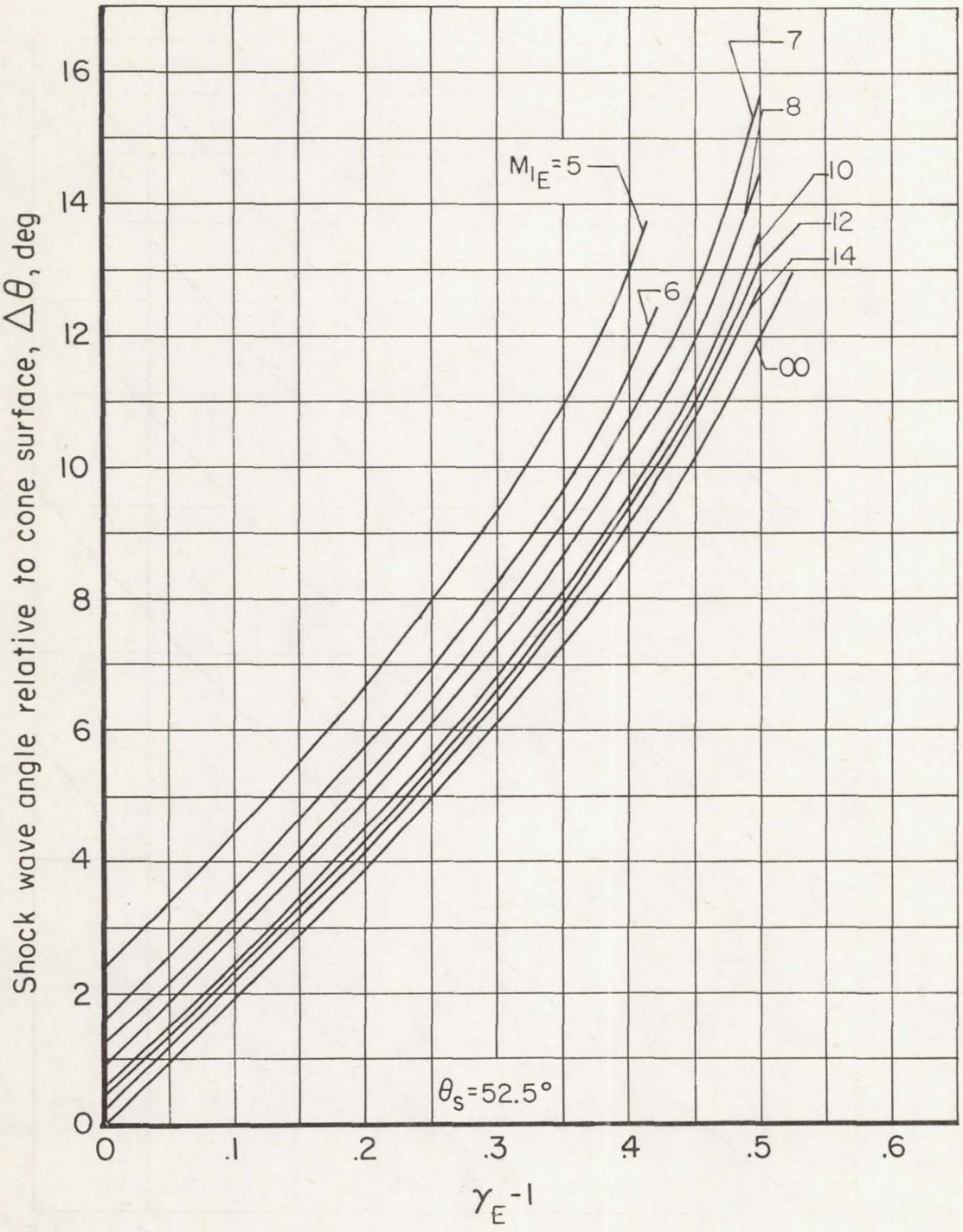

Figure 4.- Graph relating incremental shock wave angle, effective γ, and effective Mach number; $\theta_s = 52.5^\circ$.

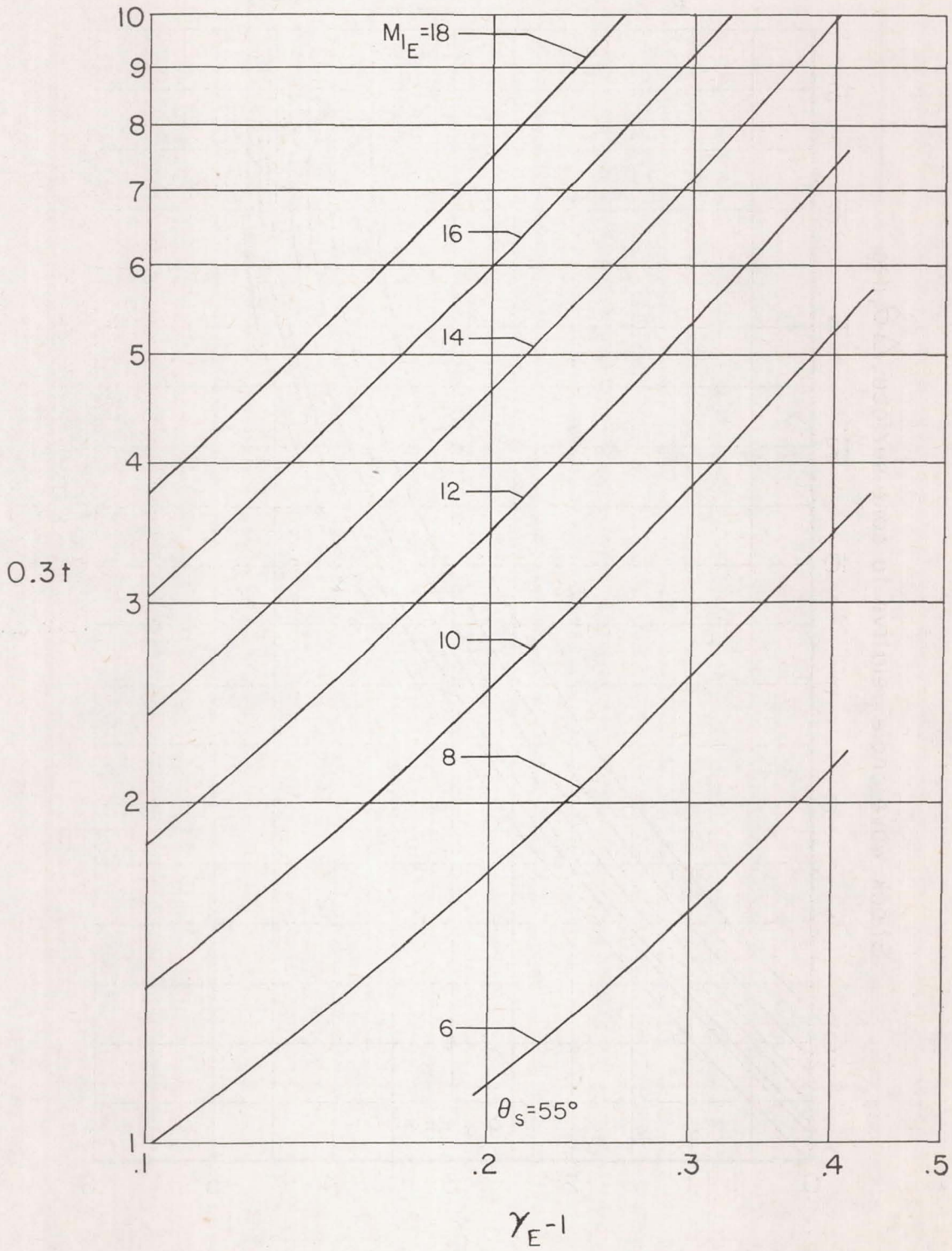

Figure 5.- Graph relating temperature ratio t, effective γ, and effective Mach number; $\theta_s = 55^\circ$.

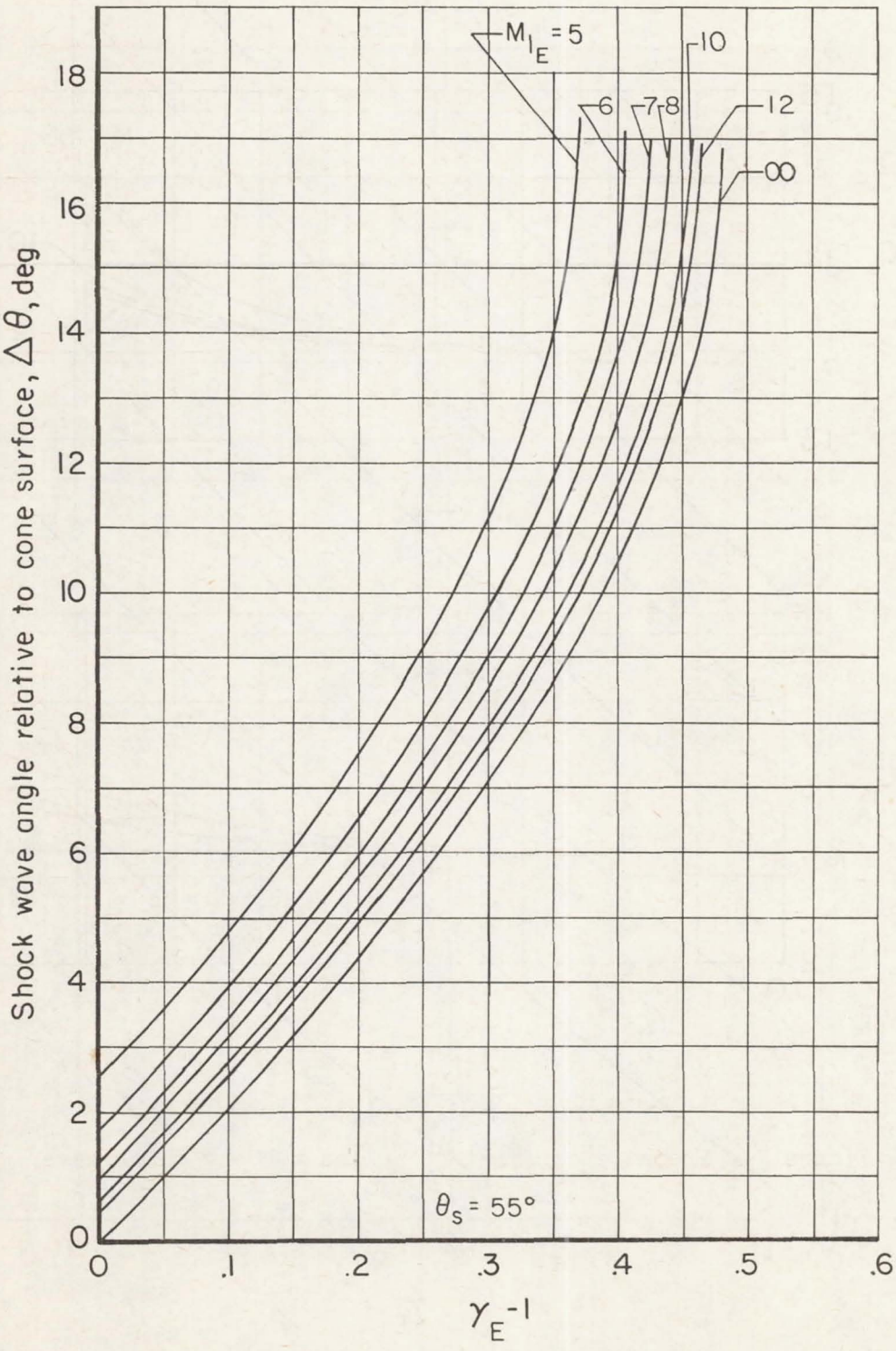

Figure 6.- Graph relating incremental shock wave angle, effective γ, and effective Mach number; $\theta_s = 55°$.

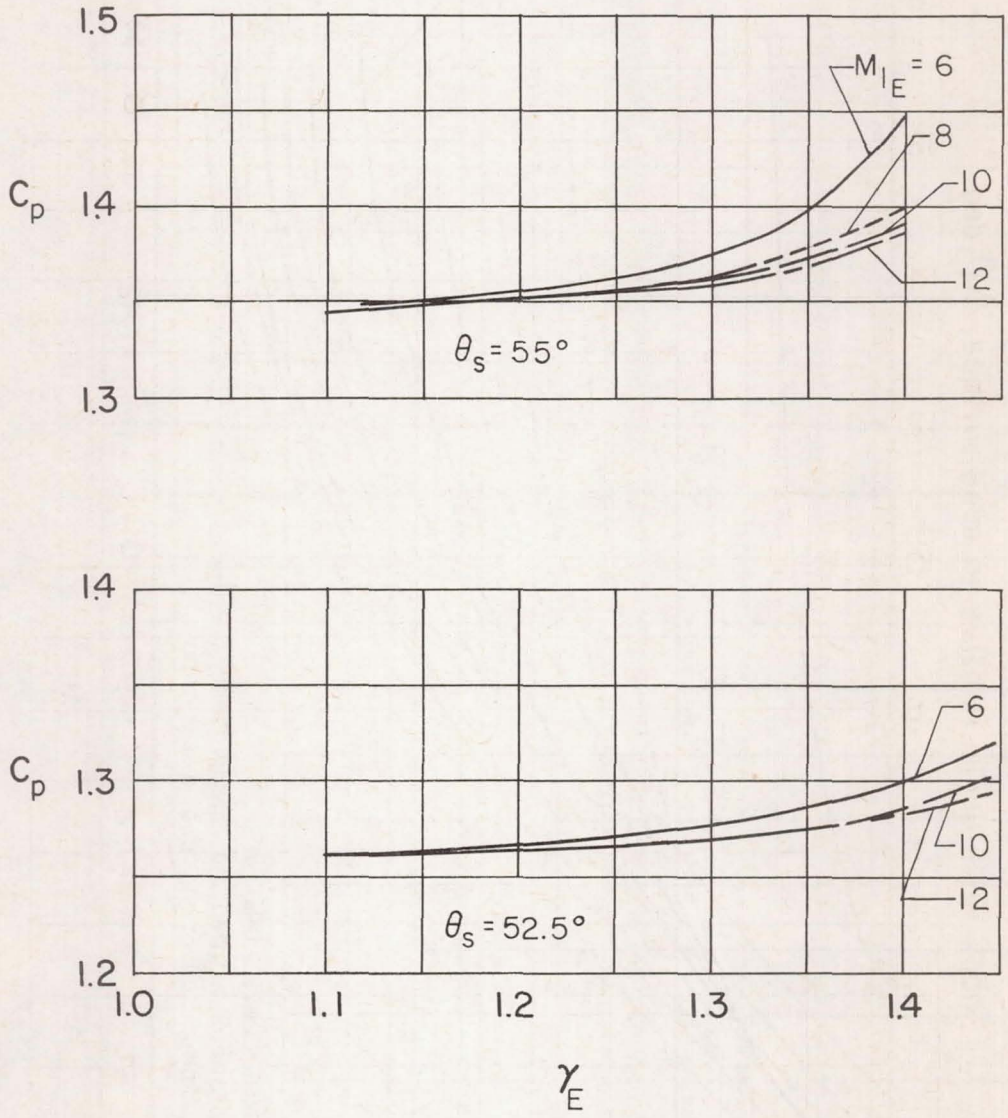

Figure 7.- Pressure coefficient behind the bow shock wave.

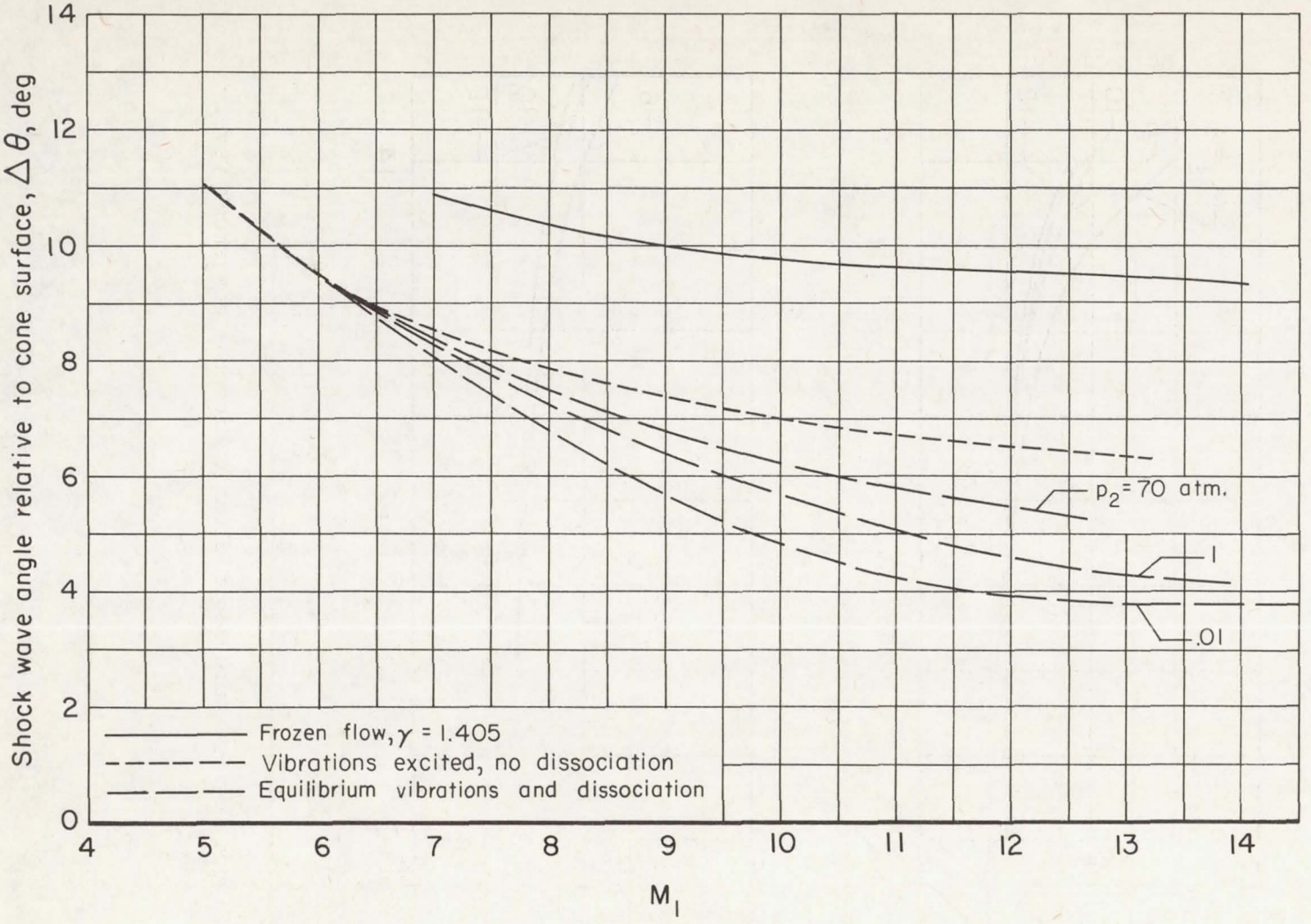

Figure 8.- Calculated incremental bow shock wave coordinate angles for frozen and equilibrium flow in air; $\theta_s = 52.5^\circ$, $T_1 = 540^\circ$ R.

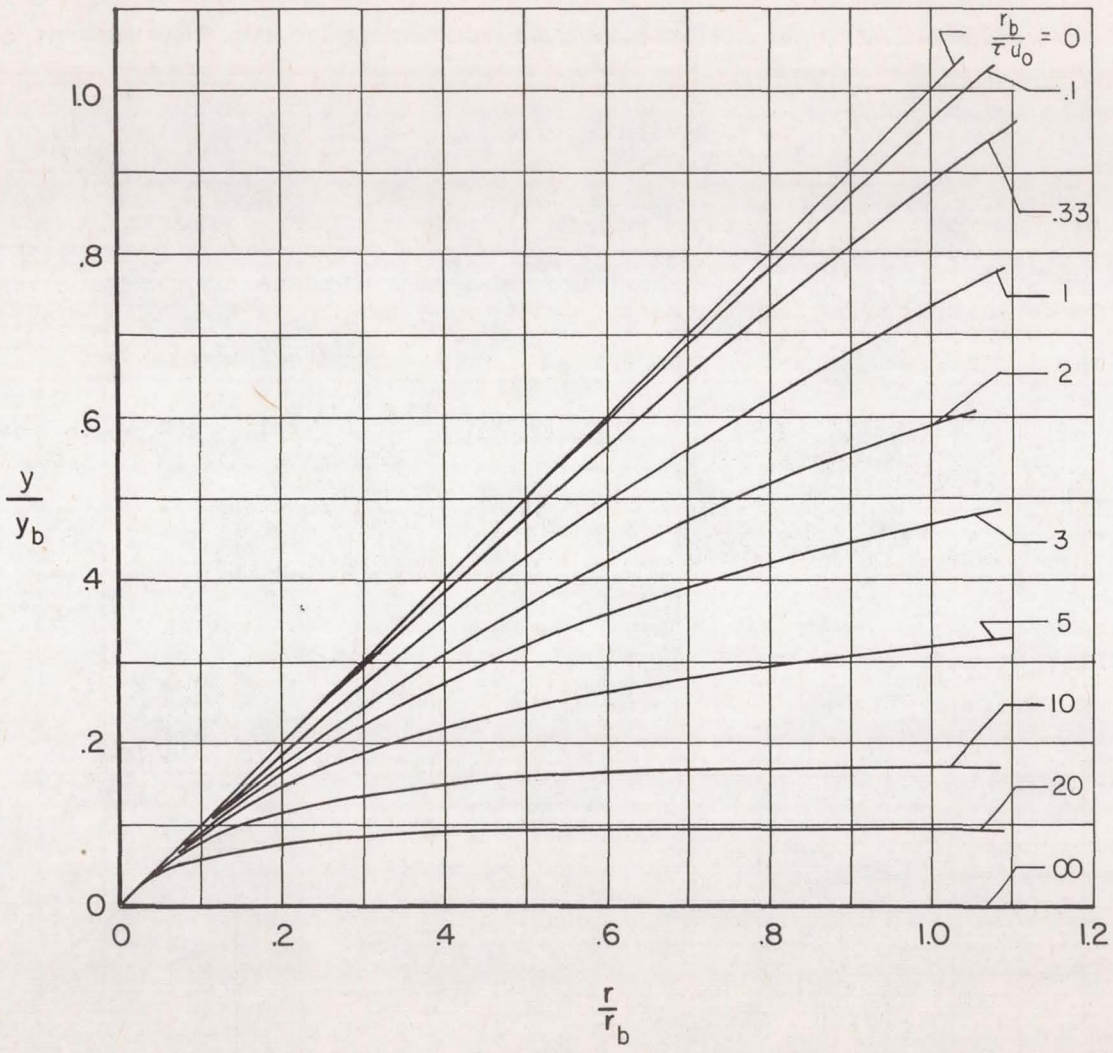

Figure 9.- The distance between the bow shock wave in nonequilibrium flow and the equilibrium-flow shock wave.

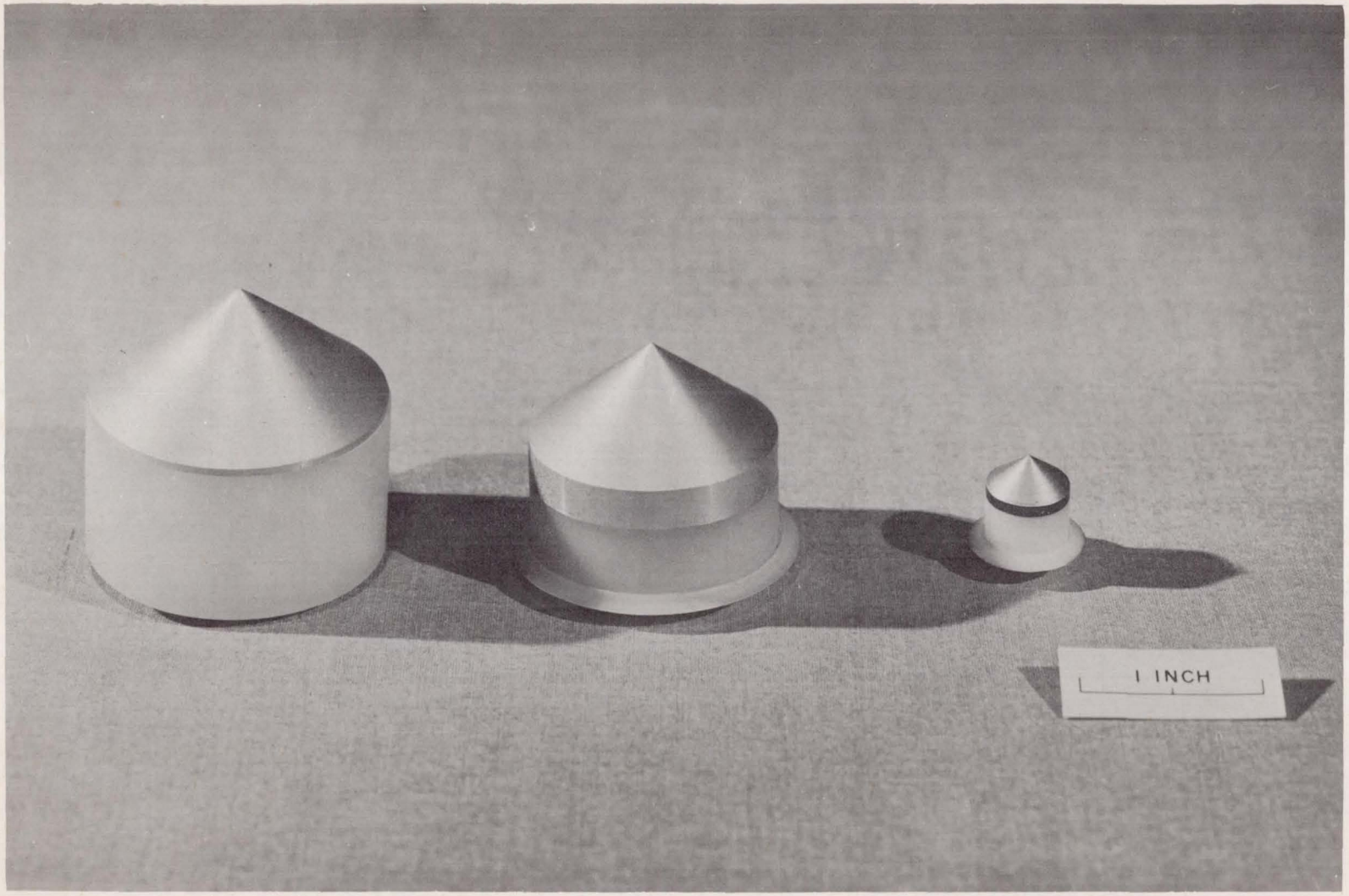

A-24887

Figure 10.- Photograph of three cone-cylinder models used in free-flight tests.

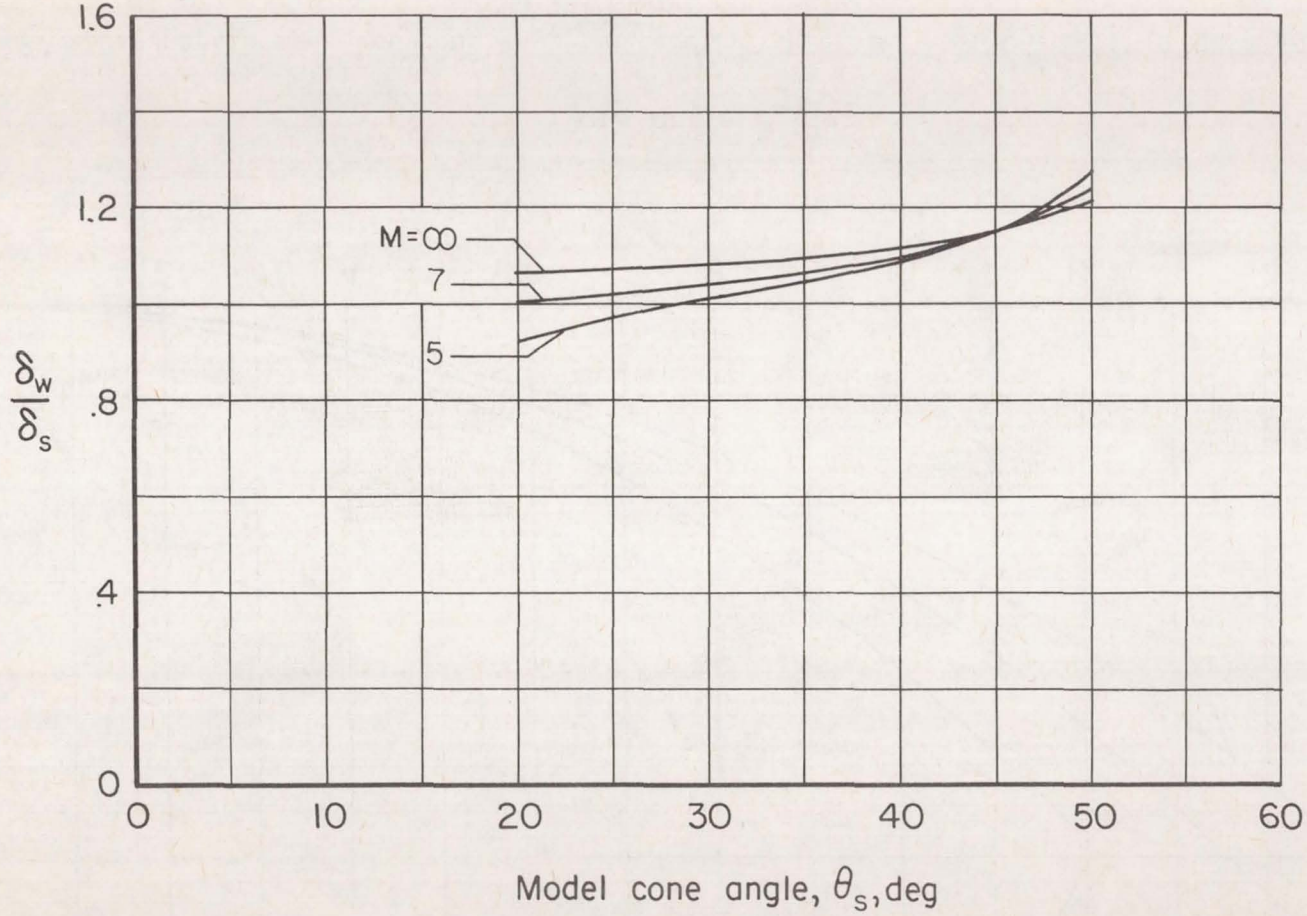

Figure 11.- The ratio of the yaw angle of the conical shock axis to the yaw angle of the solid cone; $\gamma = 1.405$.

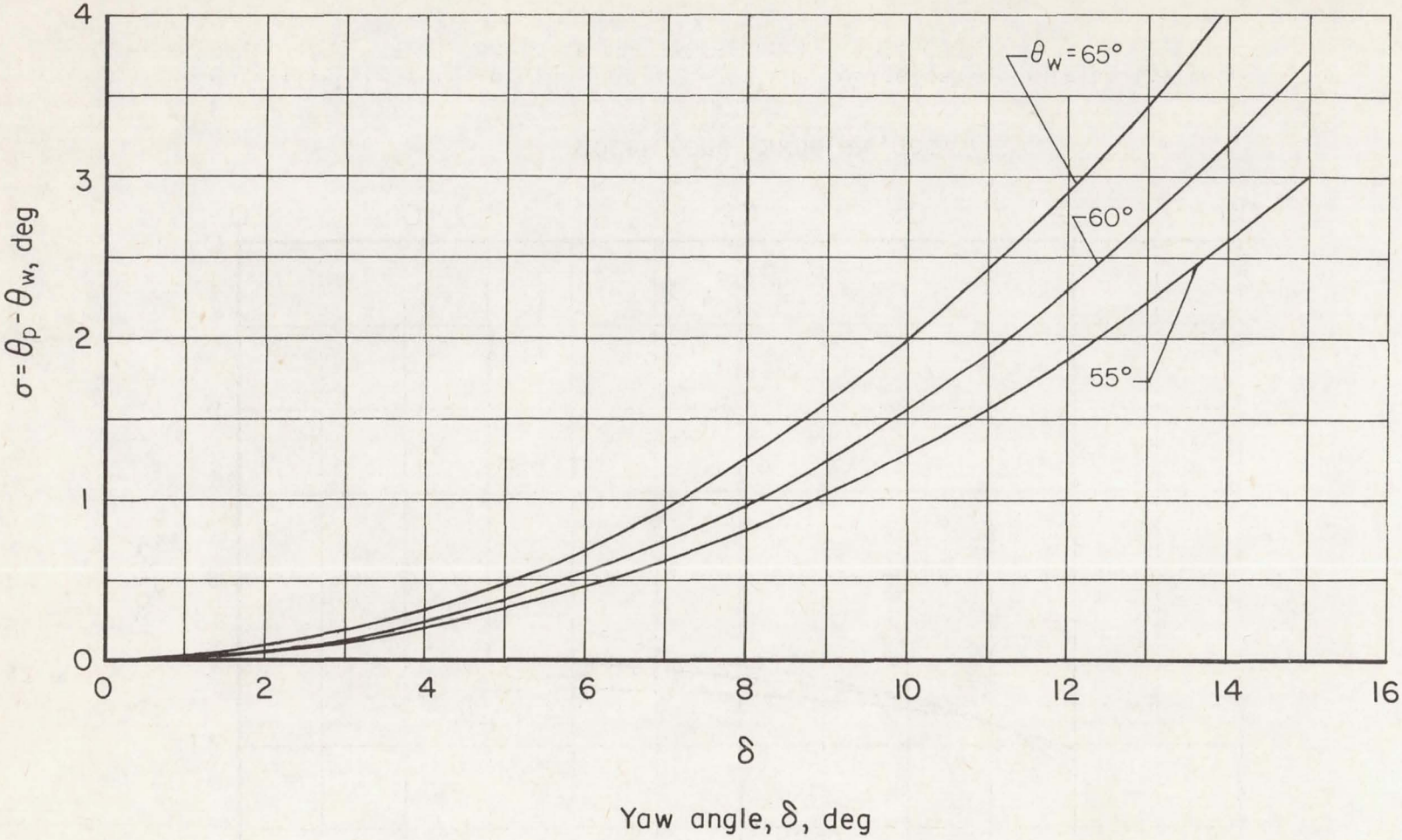

Figure 12.- Increase in apparent cone angle of the bow shock wave as a result of yaw angle of the conical shock wave axis.

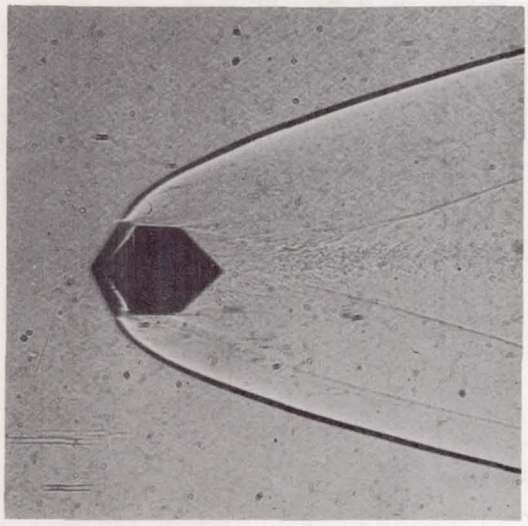

M = 6.53.

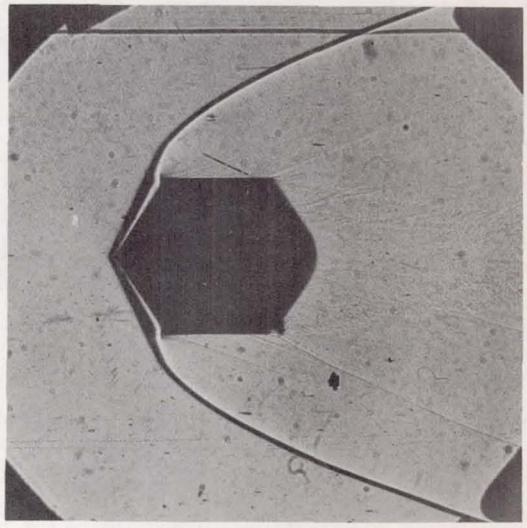

M = 7.24.

(a) Still air tests.

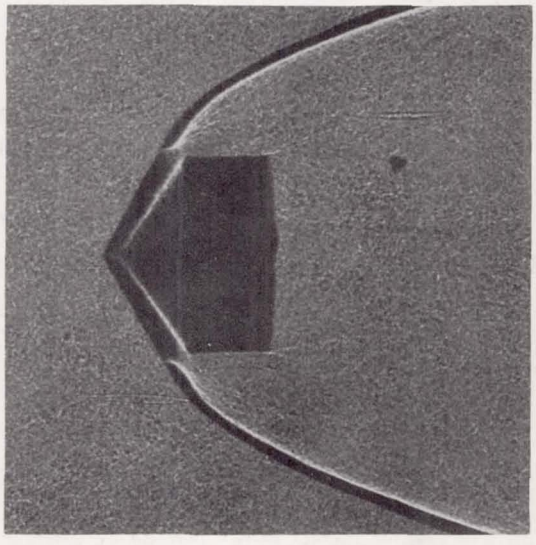

(b) Supersonic air stream; M = 10.99.

Figure 13.- Typical shadowgraphs of cone-cylinder models in free flight.

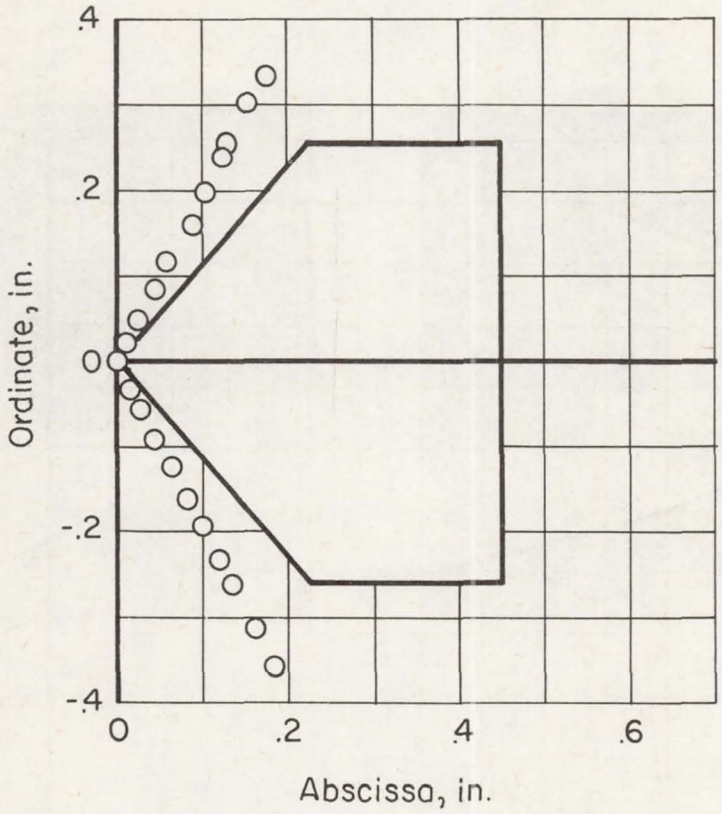

(a) Rectangular coordinates of shock wave.

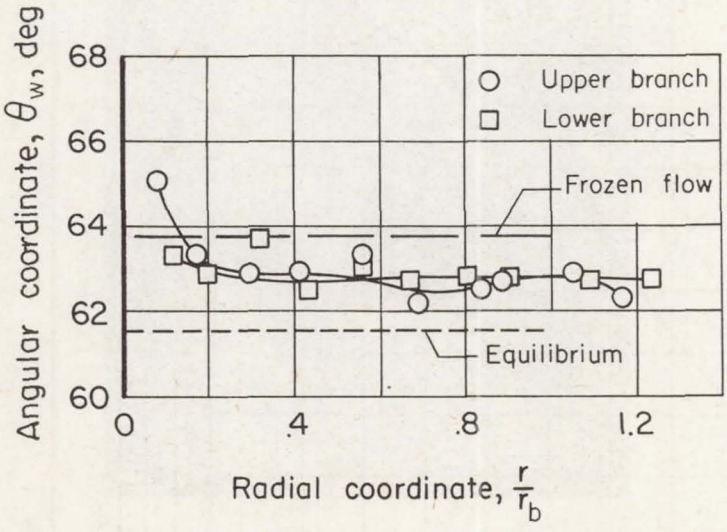

(b) Polar coordinates of shock wave.

Figure 14.- Example of bow shock wave plotted from shadowgraph data; $\theta_s = 52.5^{\circ}$, $M_1 = 6.53$.

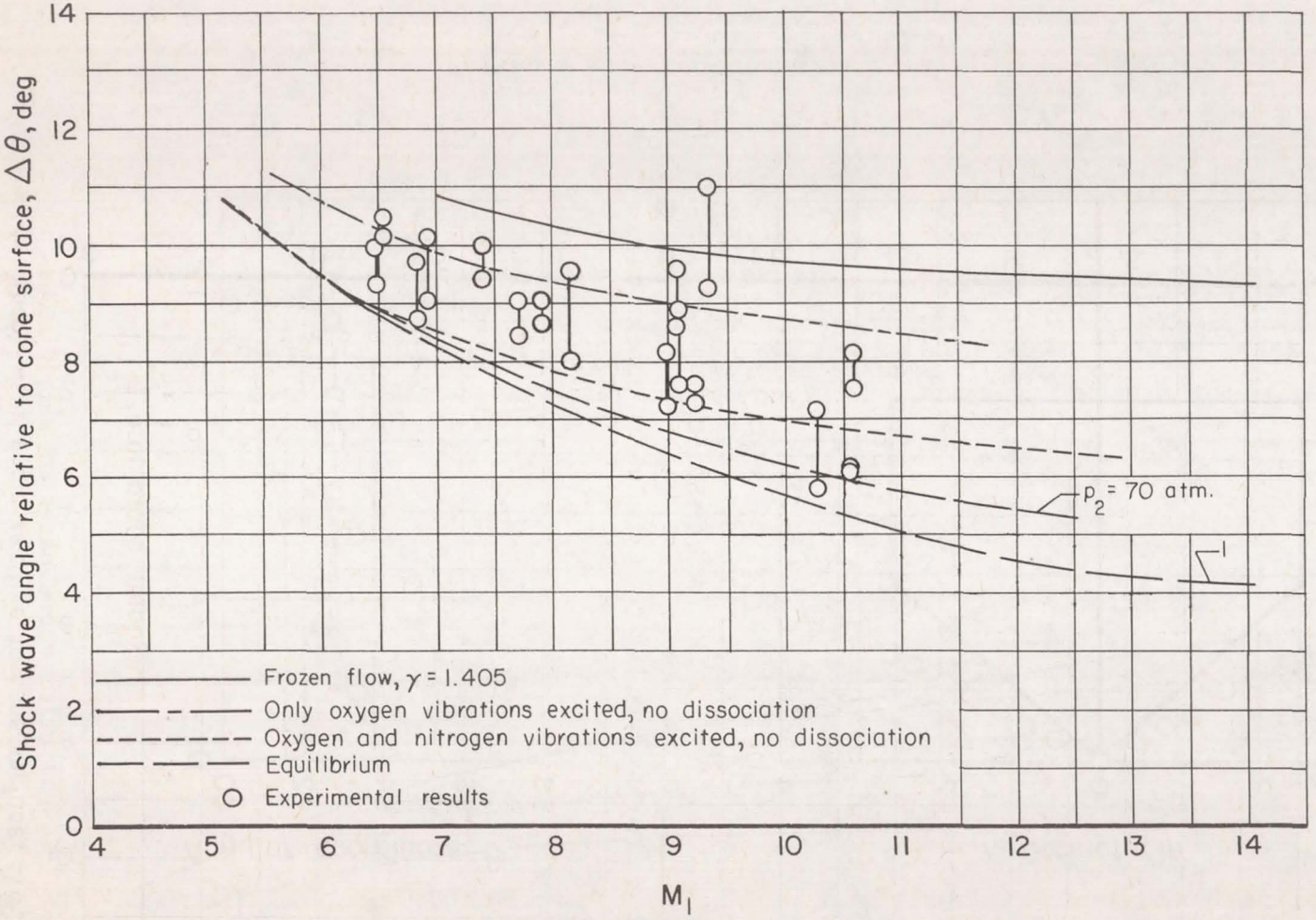

(a) $\theta_s = 52.5^\circ$; $T_1 = 540^\circ$ R.

Figure 15.- Comparison of the experimental and theoretical incremental bow shock wave coordinate angles for frozen and equilibrium flow.

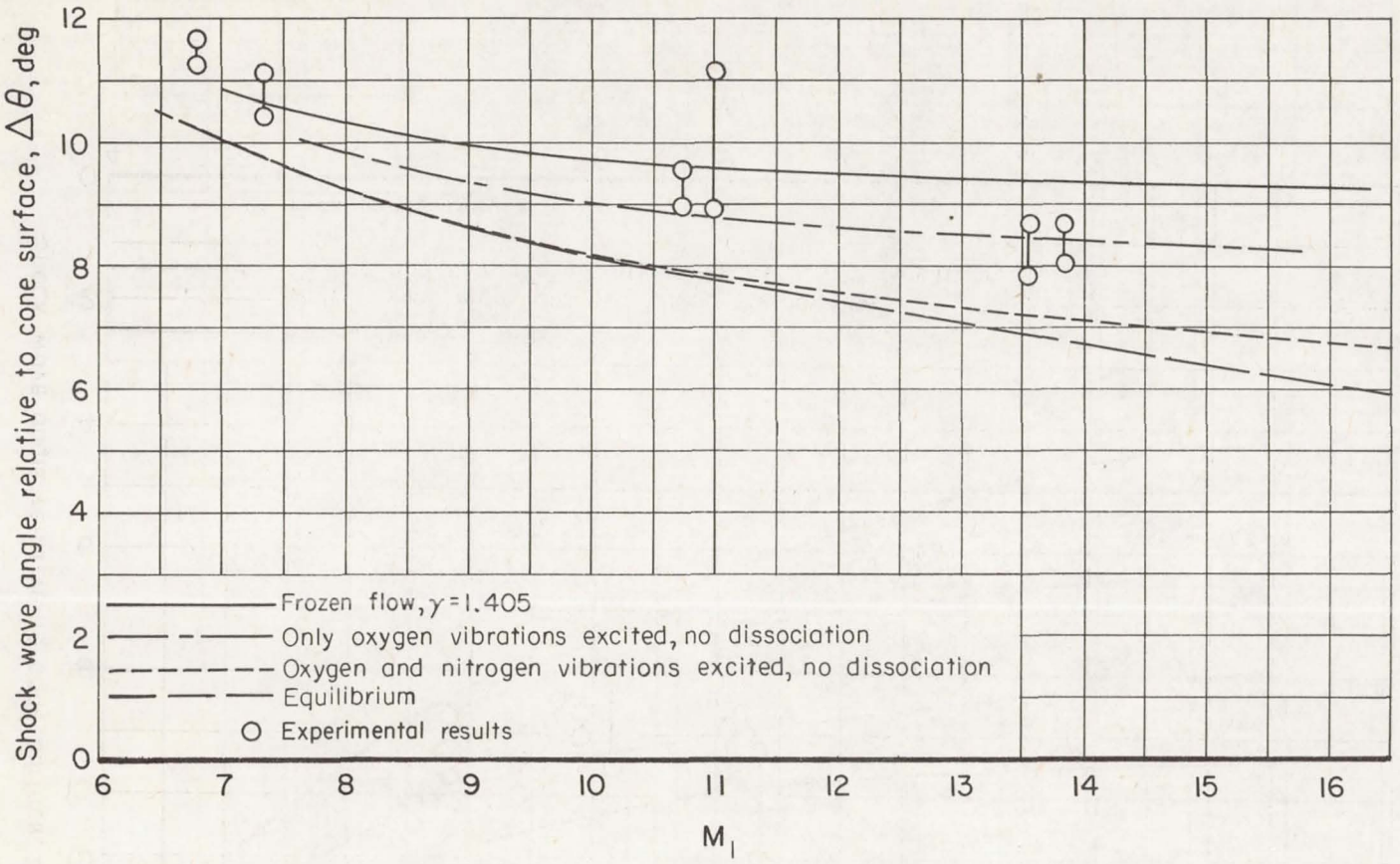

(b) $\theta_s = 52.5^\circ$; $T_1 = 193^\circ$ R

Figure 15.- Continued.

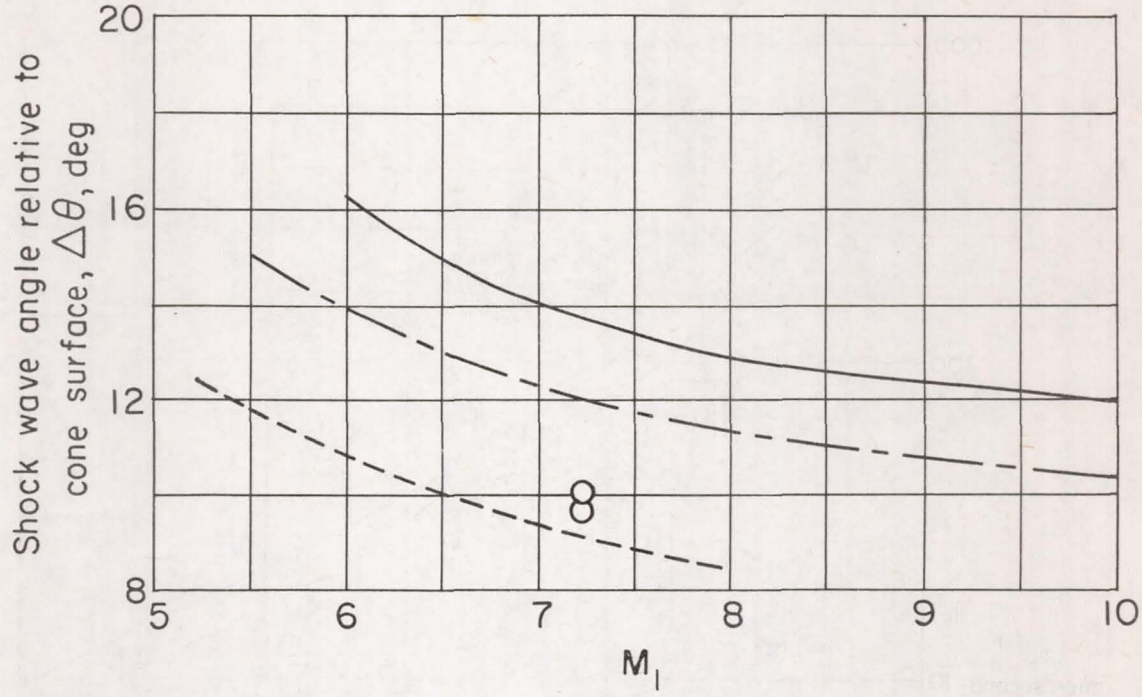

(c) $\theta_s = 55^\circ$; $T_1 = 540^\circ$ R

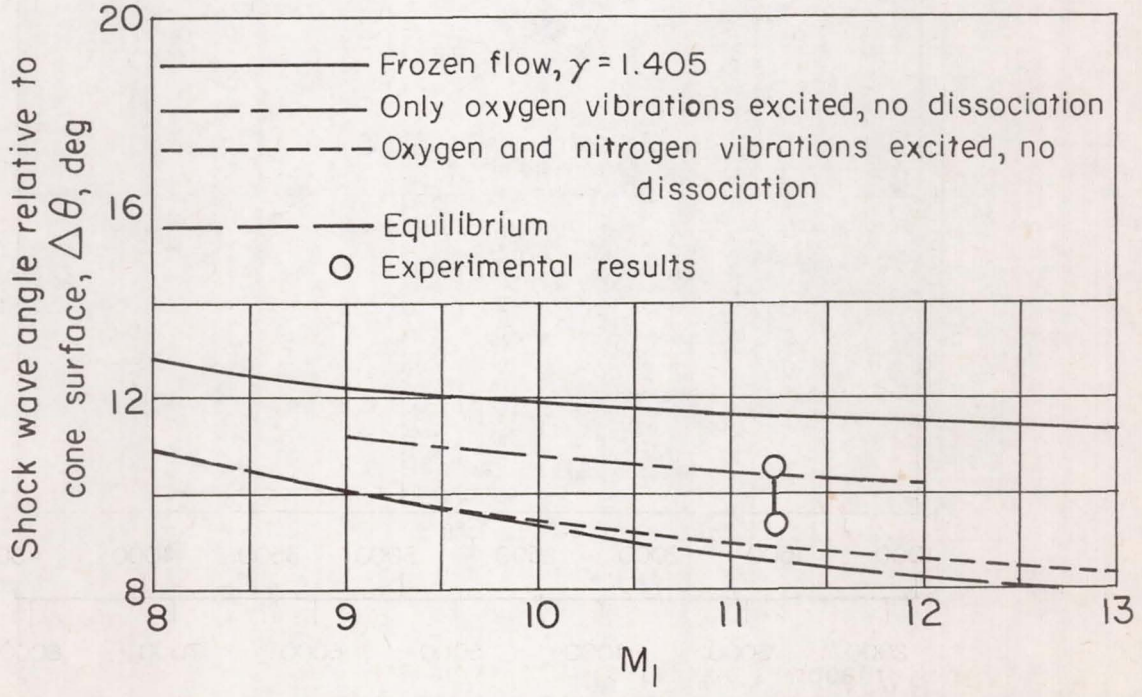

(d) $\theta_s = 55^\circ$; $T_1 = 193^\circ$ R

Figure 15.- Concluded.

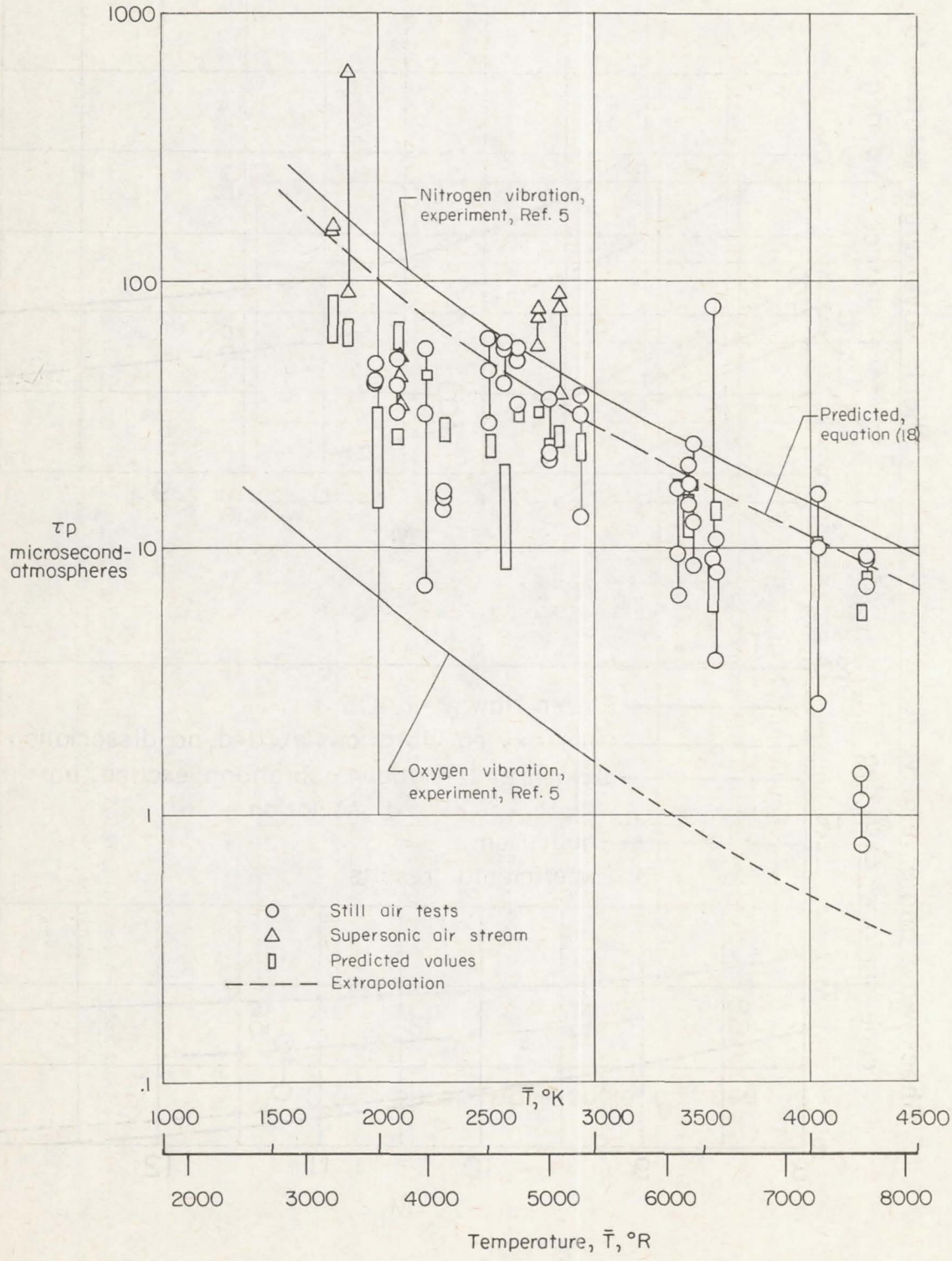

Figure 16.- Apparent relaxation time parameter as a function of average temperature behind the shock wave.

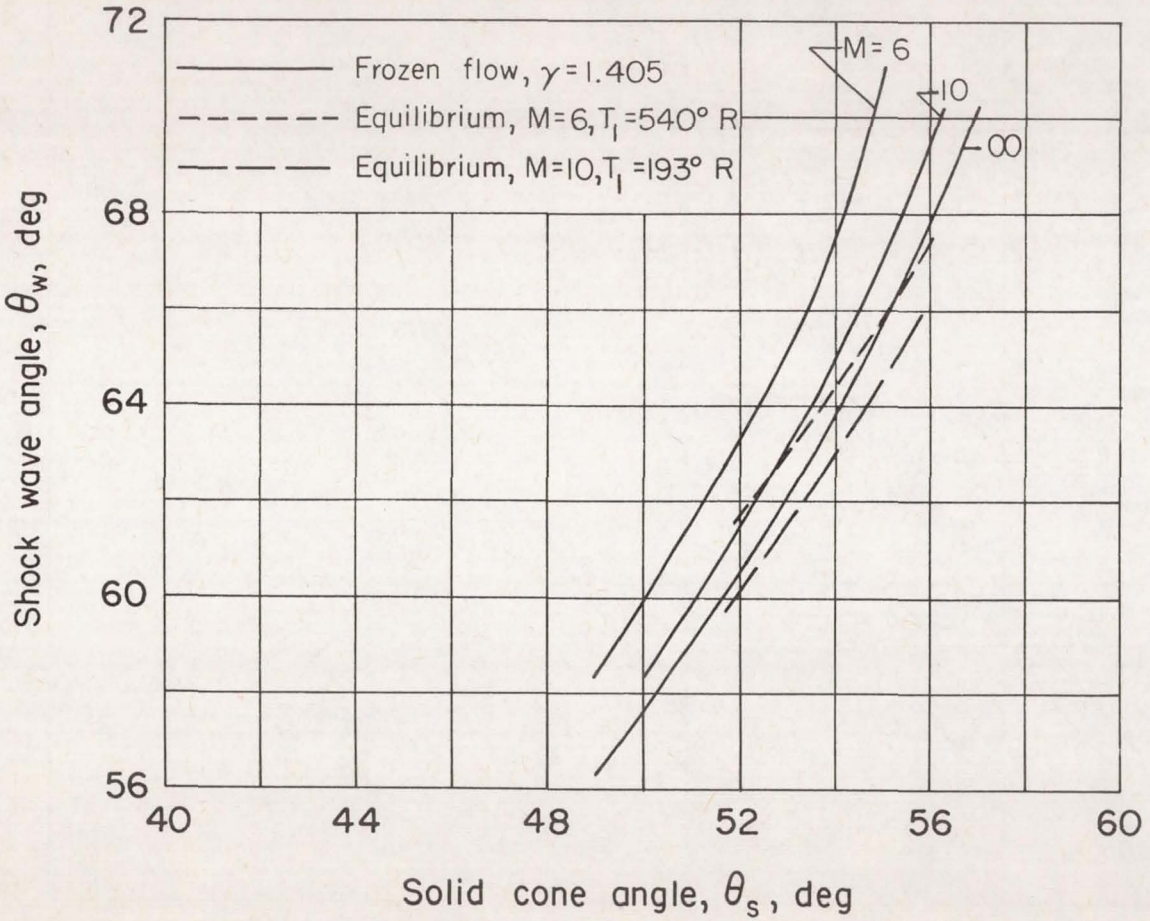

Figure 17.- Variation of bow shock wave angle with solid cone angle for various Mach numbers and free-stream temperatures.